



저작자표시-비영리-변경금지 2.0 대한민국

이용자는 아래의 조건을 따르는 경우에 한하여 자유롭게

- 이 저작물을 복제, 배포, 전송, 전시, 공연 및 방송할 수 있습니다.

다음과 같은 조건을 따라야 합니다:



저작자표시. 귀하는 원저작자를 표시하여야 합니다.



비영리. 귀하는 이 저작물을 영리 목적으로 이용할 수 없습니다.



변경금지. 귀하는 이 저작물을 개작, 변형 또는 가공할 수 없습니다.

- 귀하는, 이 저작물의 재이용이나 배포의 경우, 이 저작물에 적용된 이용허락조건을 명확하게 나타내어야 합니다.
- 저작권자로부터 별도의 허가를 받으면 이러한 조건들은 적용되지 않습니다.

저작권법에 따른 이용자의 권리는 위의 내용에 의하여 영향을 받지 않습니다.

이것은 [이용허락규약\(Legal Code\)](#)을 이해하기 쉽게 요약한 것입니다.

[Disclaimer](#)

Ph. D. DISSERTATION

**DEGRADATION ANALYSIS AND LIGAND
SUBSTITUTION METHOD FOR STABILITY
ENHANCEMENT OF InP QUANTUM DOT
LIGHT-EMITTING DIODES**

인화인듐 양자점 발광 다이오드의 안정성 향상을
위한 열화 분석 및 리간드 치환 방법

BY

KYUNGHWAN KIM

FEBRUARY 2023

DEPARTMENT OF
ELECTRICAL AND COMPUTER ENGINEERING
COLLEGE OF ENGINEERING
SEOUL NATIONAL UNIVERSITY

**DEGRADATION ANALYSIS AND LIGAND
SUBSTITUTION METHOD FOR STABILITY
ENHANCEMENT OF InP QUANTUM DOT
LIGHT-EMITTING DIODES**

인화인듐 양자점 발광 다이오드의 안정성 향상을 위한 열화
분석 및 리간드 치환 방법

지도교수 곽 정 훈

이 논문을 공학박사 학위논문으로 제출함

2023년 2월 서울대학교 대학원

전기정보 공학부

김 경 환

김경환의 공학박사 학위논문을 인준함

2023년 2월

위 원 장 : 홍 용 택 (인)

부위원장 : 곽 정 훈 (인)

위 원 : 이 재 상 (인)

위 원 : 노 정 균 (인)

위 원 : 이 현 호 (인)

Abstract

DEGRADATION ANALYSIS AND LIGAND SUBSTITUTION METHOD FOR STABILITY ENHANCEMENT OF InP QUANTUM DOT LIGHT-EMITTING DIODES

KYUNGHWAN KIM

**DEPARTMENT OF ELECTRICAL AND
COMPUTER ENGINEERING
COLLEGE OF ENGINEERING
SEOUL NATIONAL UNIVERSITY**

Recently, the interest on colloidal quantum-dot light-emitting diodes (QLEDs) for lighting and display applications have been growing due to the novel material properties of high color purity, ease of color control and process simplicity. For many years, the device fabrication processes, the device performances of QLEDs have been developed substantially by several efforts on material synthesis, electrophysical analysis and device design. Due to the advantageous characteristics for the optoelectronics application, many researches with environmentally friendly materials that do not contain heavy metals and its devices are in progress. As the performance

of heavy metal-free quantum dot (QD) is enhanced, understanding of degradation mechanism while operation is become crucial issue for stable device fabrication. Despite the numerous reports about improvement efficiency of heavy metal-free QLEDs, the mechanism of luminance deterioration is still insufficiently elucidated.

First, we analyzed early-stage luminance drop of InP/ZnSe/ZnS based QLEDs which have hybrid inverted structure. In order to classify various degradation factor that occur during operation, we intentionally fabricated devices with charge imbalance and compare the cause of degradation. To make the charge imbalance devices, we inserted the insulating layer using Poly (Methyl Methacrylate) (PMMA) before and after quantum dots (QDs) layer deposition. In aspect of reversible factors, non-radiative auger recombination was considered to be main cause by excessive electron injection. On the other hand, excessive hole transport did not affect the temporary luminance decrease, rather formulated a defect sites on QDs causing a permanent luminance drop. Conclusively, we clarify that each excess carrier can cause early-stage device degradation with different mechanism.

Second, based on the fact that excess hole state causes the severe permanent luminance drop, the stability was greatly improved by treating the QD surface through amine ligand substitution. Ligands on the QD surface not only control the synthesis process and bring the QD into a colloidal state, but also affect the electrical properties of the surface. In this experiment, we replaced the oleic acid ligand attached to the quantum dot surface to amine ligand. After ligand substitution, it was confirmed that the QD energy level was upshifted through UPS measurement. And carrier only devices show the electron injection was reduced by a small amount and hole injection was increased 4 times. As a result, current density and luminance of QLED were increased and the efficiency roll-off was improved due to the effect of enhanced hole injection without changing the spectrum through ligand substitution. Above all, QDs

degradation by electrical operation which is major cause of permanent luminance drop is enhanced and it verified through transient photoluminescence (TRPL) measurement. Furthermore, ligand exchange method effectively enhanced device stability not only red-color but also green-color. Therefore, we revealed the amine based ligand exchange can improve electrical stability of InP based QDs.

In this thesis, we studied the operational instability of InP QLED and the phenomenon that occurs through ligand substitution. Our research can contribute to the development of high stability non-heavy metal-based QLEDs.

Keywords: Quantum Dot Based Light-Emitting Diodes, Indium phosphide Quantum Dot, Ligand modification, Device stability.

Student Number: 2016-20867

Contents

Abstract	i
Contents	iv
List of Figures	viii
List of Tables	xi
Chapter 1. Introduction	1
1.1 Quantum Dot Light-Emitting Diodes	1
1.2 Non-Heavy Metal Contained QLED.....	5
1.3 Outline of Thesis.....	9
Chapter 2. Experiment Methods	11
2.1 Materials	11
2.1.1 Synthesis of ZnMgO Nanoparticles.....	11
2.1.2 Preparation of Precursors for InP Quantum Dots.....	11
2.1.3 Synthesis of Red-color InP/ZnSe/ZnS Quantum Dots..	12
2.1.4 Synthesis of Green-color InP/ZnSe/ZnS Quantum Dots	13

2.1.5	Surface Ligand Modification of the Quantum Dots.....	13
2.2	Device Fabrication.....	15
2.3	Device Characterization of Quantum Dot Light-Emitting Diodes	15
2.3.1	Current-Voltage-Luminance Measurement	15
2.3.2	Efficiency Calculation Methods.....	18
2.3.3	Operation Lifetime	18
2.4	Other Characterization Methods	20
2.4.1	UV-Visible Absorption	20
2.4.2	Photoluminescence.....	20
2.4.3	Time-Resolved Photoluminescence	20
2.4.4	Transmission Electron Microscopy	20
2.4.5	Scanning Electron Microscopy	21
2.4.6	Fourier Transform Infrared Spectroscopy.....	21
2.4.7	Atomic Force Microscopy	21
2.4.8	Ultraviolet Photoelectron Spectroscopy	21
2.4.9	Thermo Gravimetric Analysis	21

Chapter 3. Analysis on Operational Degradation of InP based QLED **22**

3.1 Characteristics of QLEDs Under Excess Carrier State **24**

3.2 Degradation Analysis Depending on Type of Luminance Drop..... **29**

3.3 Origin of Temporary Degradation..... **32**

3.4 Origin of Permanent Degradation **24**

3.5 Summary..... **39**

Chapter 4. Stability Enhancement of QLED via Ligand Exchange Method **40**

4.1 Ligand Exchange of InP/ZnSe/ZnS QDs **42**

4.2 Effect of Ligand Exchange on Device Characteristics **47**

4.3 Versatility in Improving the Stability by Ligand Exchange Strategy..... **54**

4.4 Summary..... **59**

Chapter 5. Conclusion	60
Bibliography	62
Publication	67
한글 초록	70

List of Figures

Figure 1.1 (a) The development of display industry. (b) A size controllable color change of QDs. (c) comparison of R, G, B QLEDs (solid lines) and those of OLEDs. (dashed lines) (d) International commission on illumination (CIE) chromaticity diagram for qualifying the quality of display, TVs, and other devices. (e) Schematic illustration of solution-based inkjet printing.....	3
Figure 1.2 Previous studies about red InP/ZnSe/ZnS based (upper) and green InP/ZnSe/ZnS based QLED (lower)	6
Figure 2.1 The CIE standard observer color matching functions.....	17
Figure 3.1 Absorption and normalized PL spectra with a TEM image of InP/ZnSe/ZnS QDs.....	24
Figure 3.2 Schematic illustration of inverted QLEDs with a cross-section TEM image.	25
Figure 3.3 Schematic energy diagram of the (a) pristine, (b) hole-excess, and (c) electron-excess devices.....	25
Figure 3.4 J–V characteristics of single carrier devices without and with a PMMA layer. The structure of the HOD is ITO/MoOx (10 nm)/PMMA (0 or 10 nm)/TCTA (50 nm)/MoOx (10 nm)/Al, and that of the EOD is ITO/ZMO (40 nm)/PMMA (0 or 10 nm)/Al.	27
Figure 3.5 Devices characteristics in terms of (a) J–V–L, (b) current efficiency, (c) operational lifetime, and (d) EL spectra.	28

Figure 3.6	Operational lifetime of the (a) pristine, (b) hole-excess, and (c) electron-excess devices with discharging every 15 min. The difference of the (d) permanent and (e) temporary degradation in each cycle. The inset image shows how to obtain the values.	31
Figure 3.7	TRPL curve of device (blue line: TRPL of QD in solution state)	32
Figure 3.8	Temperature change during electrical operation of (a) pristine (b) hole excess (c) electron excess devices	33
Figure 3.9	AFM image of (a) ZnO/QD, (b) ZnO/PMMA/QD, (c) ZnO/QD/PMMA	33
Figure 3.10	TRPL decay curves of the (a) pristine, (b) hole-excess, and (c) electron-excess QLEDs, and the (d) EOD, (e) HOD, and (f) HOD with a PMMA spacer layer, measured at 15-min intervals.	36
Figure 3.11	J–V characteristics of HOD before and after degradation.....	38
Figure 4.1	FT-IR measurement of oleic acid and hexyl amine ligand QDs	43
Figure 4.2	TGA result of (a) zinc oleate and (b) QDs with OA and HA ligand	43
Figure 4.3	Ultraviolet photoelectron spectroscopy and schematic energy diagram of QD	44
Figure 4.4	(a) Absorbance, PL spectrum and (b) TRPL decay of oleic acid and hexyl amine ligand QDs in solution state	45
Figure 4.5	AFM image of (a) Oleic acid QD (b) Hexyl amine QD film inset of (a) and (b) represent SEM image of QD film	46
Figure 4.6	Comparison of the performance of QLEDs with OA and HA ligands, in terms of (a) J–V, (b) L–V (c) current efficiency, and (c) EL spectrum	48

Figure 4.7	(a) Comparison of the performance of QLEDs with OA and HA ligands, in terms of operational lifetime. (b) Relative luminance with discharging and the permanent and temporary degradation at 15-min intervals of (c) OA (d) HA device	50
Figure 4.8	TRPL decay of (a) oleic acid ligand QD device and (b) hexyl amine ligand QD device before and after 1 hour degradation	51
Figure 4.9	Operation time dependent nyquist plot of (a) oleic acid ligand QLED (b) hexyl amine ligand QLED	53
Figure 4.10	(a) FT-IR measurement of green InP QDs	54
Figure 4.11	(a) Absorbance, PL spectrum and (b) TRPL decay of green oleic acid and hexyl amine ligand QDs in solution state	56
Figure 4.12	(a) UPS measurement of oleic acid and hexyl amine ligand green InP QDs. (b) Schematic energy diagram of QDs and TCTA	56
Figure 4.13	Comparison of the performance of green-color InP/ZnSe/ZnS QLEDs with OA and HA ligands, in terms of (a) J–V–L, (b) current efficiency, (c) operational lifetime, and (d) normalized EL spectrum.	58

List of Tables

Table 3.1 TRPL decay time in QLEDs and single-carrier devices.	37
---	----

Chapter 1

Introduction

1.1 Quantum Dot Light-Emitting Diodes

As the nanocrystalline semiconductor, quantum dots (QDs) exhibit unique properties due to their small size. Distinct characteristics, such as size-tunable bandgap engineering, high photoluminescence quantum yield (PL QY), and narrow full-width at half-maximum (FWHM) have made QDs practically adoptable in light sources, lasers, solar cells, photodetectors and biomarkers. [1-10] Especially, high PL QY close to unity and narrow spectral emission of QDs enabled them to be used as bright and efficient emitters in optoelectronic devices. [11-14] Therefore, QD is spotlighted as a next-generation display material in the rapidly developing optoelectronic industry. (Figure 1.1(a)) As shown in figure. 1.1(b), a photographical image denotes the size-dependent bandgap tunability of QDs and bandgap tunability by size control. Superior to OLEDs, FWHM of QLEDs has narrow bandwidth less than 30 nm. Figure 1.1(c) shows the difference of FWHM between Cd-based QLEDs

and typical OLEDs, which are wider bandwidth due to the vibronic states in organic dyes. Furthermore, the narrow bandwidth and high color purity of QDs can make them wide color gamut in CIE 1931 color space as depicted in figure 1.1(d). In addition, the low device fabrication cost is an advantage since solution processing is possible. (figure. 1.1(e))

Since the first demonstration of QD based electroluminescence devices by the Colvin *et al.*, intensive efforts have been conducted to achieve high performance EL device with high external quantum efficiency (EQE) and high brightness. [15, 16] In 2014, X. Dai et al reported a highly efficient Cd-based red QLED with a low turn-on at 1.7 V and high EQE up to 20.5%. [17] The highly efficient QLEDs was achieved by inserting an insulating layer between emissive layer and oxide electron transport layer. This methodology makes this device comparable to state-of-the-art vacuum deposited QLEDs at that time. Besides, H. Moon et al. efficiently controlled the negative dipole moment using ligand modification and thus achieved a high maximum EQE (24.8%) [18]. Interestingly, J. Song et al. reported hybrid type QLEDs, exhibiting extremely high peak EQE (> 30%) and very low efficiency roll-off at high current density (150 mA cm^{-2}) [19]. These extraordinary properties are coming from not only use of a gradient core/shell composition with thicker ZnSe interlayer shell and ultrathin ZnS outer shell but also 2-ethylhexane-1-thiol (EHT) surface ligand modification. Thanks to these efforts, QLEDs are expected to be used in future applications such as mobile phone and TVs.

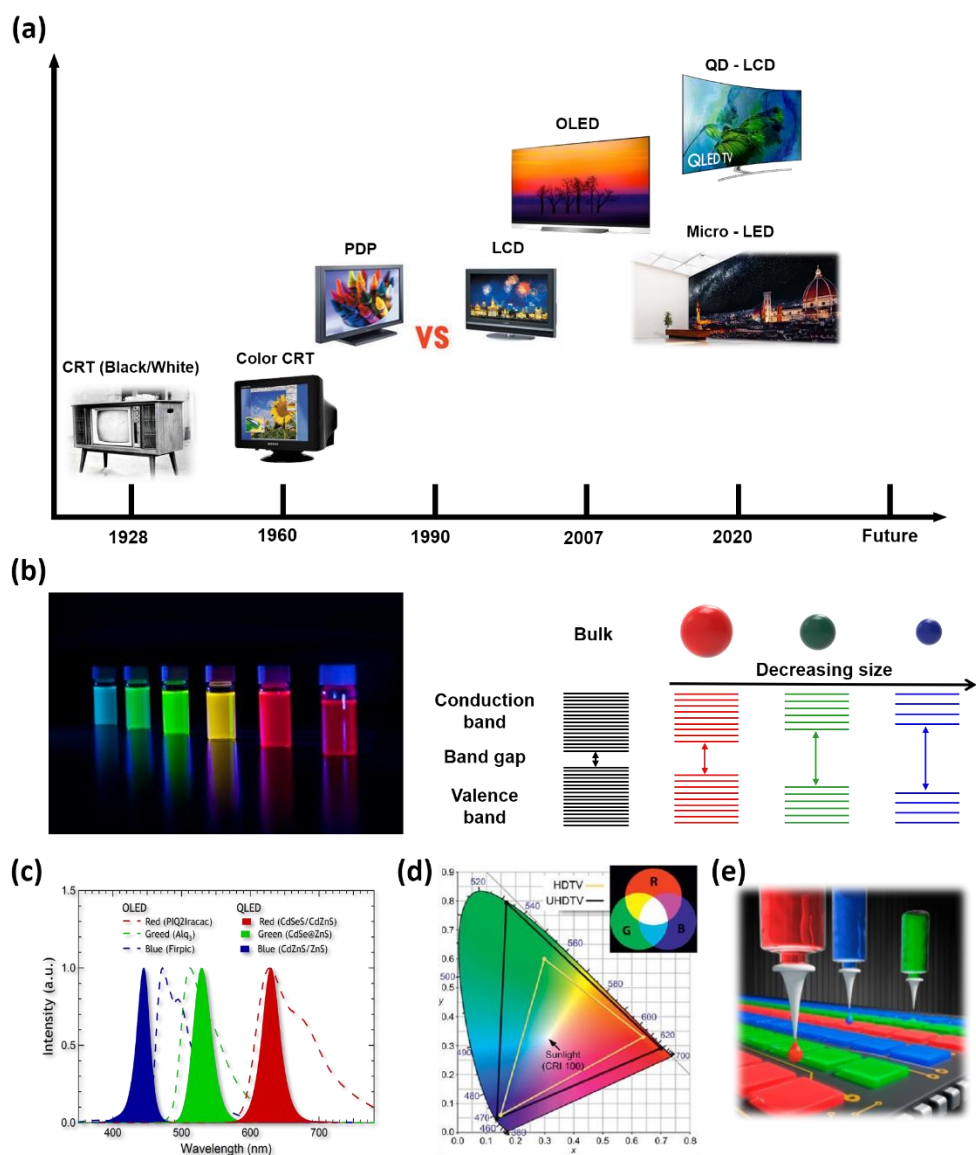


Figure 1.1 (a) The development of display industry. (b) A size controllable color change of QDs. (c) comparison of R, G, B QLEDs (solid lines) and those of OLEDs. (dashed lines) (d) International commission on illumination (CIE) chromaticity diagram for qualifying the quality of display, TVs, and other devices. (e) Schematic illustration of solution-based inkjet printing.

Along with the device performance, the operation instability of devices is also critical issues to overcome. The stability of QLED is still insufficient compared to that of commercialized OLED, and it is an important issue to be solved along with efficiency. Thus, elucidation of the degradation mechanism is key factor to improve device stability. As the external cause of QLED deterioration, oxygen and moisture act significant role on degradation of QDs material inducing generation of trap state. [20–22] The optical properties of QD can be readily altered by chemical reactions occurring on the surface because QD have a high surface area compared to their volume due to their small size. In case of operational instability, exciton energy is transferred to a nearby carrier causing non-radiative auger recombination when the certain carrier is excessively injected into a QD due to an imbalance in charge transport during device driving. [23–25] In addition, charge imbalance becomes more severe or a new quenching site is generated due to deterioration of the organic transport layer by leakage current passing through the QDs layer. [26–28] Therefore, charge balance is the essential factor when designing QLED structure. And joule heat generated by device resistance during electrical operation can affect the properties of charge transport layer and causes permanent degradation of the material when the temperature is high enough. [29, 30] Not only joule heat but also energy of carrier can induce dissociation of ligand from QDs surface causing decrement of PLQY of QDs. [31] As can be seen from the previous description, the quantum dot degradation mechanism is caused by a combination of several problems. Consequently, the degradation mechanism of QLED is a combination of several reason. Therefore, it is necessary to analyze each mechanism independently and find a suitable improvement method.

1.2 Non-Heavy Metal Contained QLED

Although the QDs are being discussed as next-generation display materials based on their excellent optical properties and stability, there are issues to overcome for limitations of material. As the penetration rate of electronic devices gradually increases, people prefer eco-friendly materials, and the awareness of excluding heavy metals harmful to the human body increases. In addition, several environmental directives and regulations gradually impose the development and use of eco-friendly substances for commercial production. [9] Therefore, it is essential to use eco-friendly materials to make products using quantum dots, and InP-based QDs are being developed to replace Cd based QDs. Among a few heavy-metal-free QD compositions, InP-based QDs have been highlighted as a promising substitute because of their descent optical properties as well as low toxicity. [32-34] With systematic investigation of mechanism and device physics and the rapid development of materials and device fabrication technologies, the electroluminescence (EL) efficiency of InP QLEDs has been greatly improved and is comparable to that of Cd-based QLEDs.

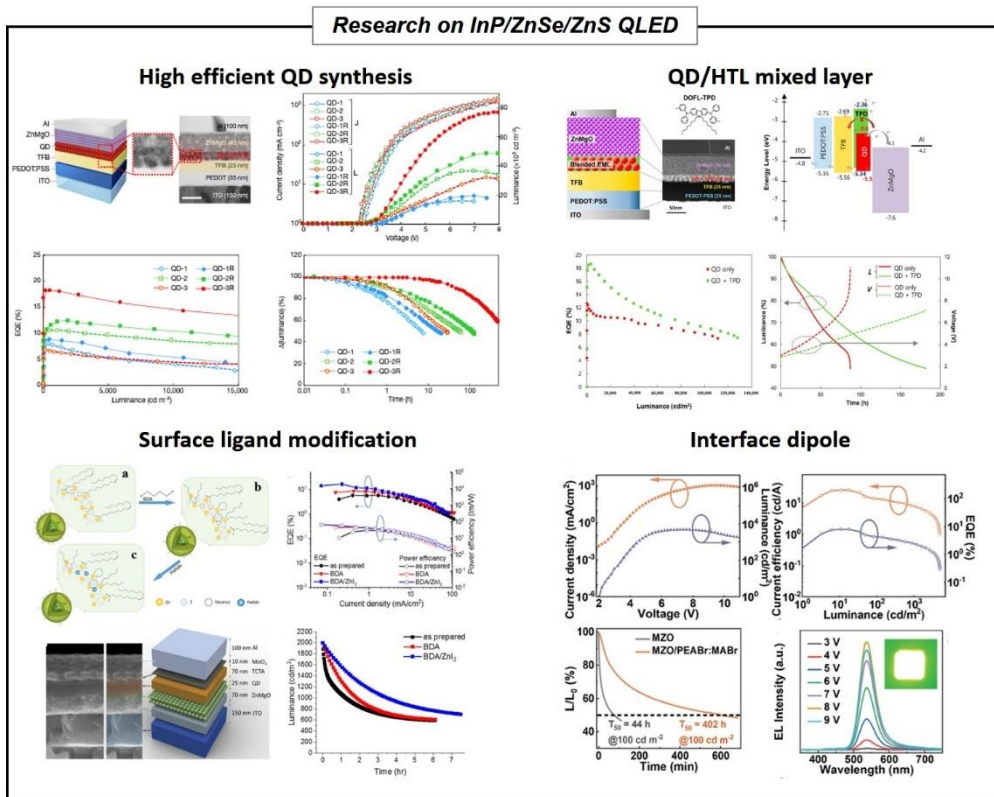


Figure 1.2 Previous studies about red InP/ZnSe/ZnS based (upper) and green InP/ZnSe/ZnS based QLED (lower)

Won et al. achieved a red InP/ZnSe/ZnS device with an external quantum efficiency (EQE) of 21.4% and an operational lifetime (100ni, LT50) over 100,000 hours by improving the synthesis process. [35] In addition, surface ligand of QDs was replaced with shorter one for the enhancement of charge injection. Han et al. achieved a red InP/ZnSe/ZnS QLED with an EQE of 18.6% and an operational lifetime over 100,000 hours by blended emission layer. [36] As they mixed the hole-transporting organic molecule with QDs without phase separation, stability of device was enhanced by suppression of electron leakage to hole transport layer. Chao et al. report green InP/ZnSe/ZnS QDs device with EQE of 16.3% and lifetime with 545 hours as

modified the surface ligand by alkyl amine and zinc halide. [37] Exchanged ligand made dipole layer toward QDs which facilitate the hole injection and enhanced charge balance of device. Wang et al. adapt the dipole layer between ZnMgO and aluminum electrode to reduce over injected electron. [38] They achieved green InP/ZnSe/ZnS device with an EQE of 7.8% and lifetime with 400 hours.

Owing to multilateral efforts to improve the performance of materials and devices, the EQE of InP-based QLEDs is now approaching the values obtained in Cd-based QLEDs. However, only a few studies have reported the operational lifetime of InP-based QLEDs and the values are still far behind that of Cd-based QLEDs. As reasons, it has been suggested that InP-based QDs possess lower uniformity in size/shape, thinner shell due to larger lattice mismatch, and inferior electron confinement, which may result in surface oxidation, Auger process, and/or charge trapping in defect states.[36,39–42] During electrical operation of QLEDs, these degradation processes are further accelerated by excess carriers due to electron–hole charge imbalance, because excess carriers tend to form negatively charged QD states (QD^-) and accumulate at the interfaces near QDs. Thus, most of previous lifetime research of InP-based QLEDs mainly focused on the improvement of charge balance. However, the effects of excess carriers on the degradation of InP-based QDs and QLEDs are not clearly revealed yet, because a variety of factors are entangled complicatedly. Therefore, it is essential to investigate how the excess carriers affect the degradation in order to further ameliorate the operational lifetime of the InP-based QLEDs. Also, to distinguish the causes and effects related to operational lifetime, systematic studies using well-designed device structures and experimental techniques are desired.

In this work, we investigate the effect of excess carriers on degradation of InP-based QLEDs by introducing a charge-imbalanced device structure that is intentionally designed to directly observe how excess holes and electrons influence

the QLED lifetime. Also, we analyzed the operational lifetime by dividing it into two components, i.e., temporary and permanent degradation which can be quickly recovered by reverse bias or not, respectively. Interestingly, the hole-excess device exhibited significant permanent degradation with little temporary luminance drop, whereas the electron-excess device showed the exact opposite degradation. In parallel, the PL decay time of QDs upon electrical stress was measured to identify the formation of non-radiative recombination sites. From the results, we infer that excess holes severely affect the formation of defect sites causing non-radiative recombination, leading to permanent degradation of QLEDs. As a method to restrain the permanent degradation, we adopted QDs with electrochemically stable ligands and verified that the irreversible degradation by excess holes was effectively suppressed.

1.3 Outline of Thesis

This thesis consists of five chapters, including the Introduction and Conclusion.

In the introduction of **Chapter 1**, an overview of InP based QLEDs and their previous research papers are briefly explained.

Chapter 2 includes material preparation: the methods used to prepare ZnMgO nanoparticles and type I InP/ZnSe/ZnS QDs used in this thesis. In addition, the characterization methods for QLEDs are summarized in this chapter, and the electrical and morphological characterization methods for thin films used in this thesis are depicted.

In **Chapter 3**, we analyzed early-stage luminance drop of InP/ZnSe/ZnS based QLEDs which have hybrid inverted structure. In order to classify various degradation factor that occur during operation, we intentionally fabricated devices with charge imbalance and compare the cause of degradation. To make the charge imbalance devices, we inserted the insulating layer using PMMA before and after QDs layer deposition. In aspect of reversible factors, non-radiative auger recombination was considered to be main cause by excessive electron injection. On the other hand, excessive hole transport did not affect the temporary luminance decrease, rather formulated a quenching site at the interface between QDs and hole transport layer causing a permanent luminance drop.

In **Chapter 4**, based on the fact that various causes of deterioration occur due to poor stability of QDs under hole excess state, the initial stability was greatly improved by treating the QD surface through amine ligand substitution. As we suspected the QDs degradation is stem from the ligand detachment formulating defect site, alkyl amine ligand which is known as electrochemically stable was applied. Through the

enhanced stability and energy shift of surface of QDs, not only early-stage lifetime but also long-range stability also enhanced.

Finally, in **Chapter 5**, we summarize our work and make concluding remarks.

Chapter 2

Experimental Methods

2.1 Materials

Indium acetate ($\text{In}(\text{Ac})_3$, 99.99%), zinc acetate ($\text{Zn}(\text{Ac})_2$, 99.99%), oleic acid (99%), 1-octadecene (ODE, 99%), tris(trimethylsilyl)phosphine ($(\text{TMS})_3\text{P}$, 99.9%), n-trioctylphosphine (TOP, 99%), n-trioctylamine (TOA, 99%), selenium (Se, 99.9%), sulfur (S, 99.9%) are purchased from Uniam. PMMA ($M_w \approx 8$ kDa), hexylamine (99%), zinc acetate dihydrate (98%), tetramethylammonium hydroxide pentahydrate (97%), magnesium acetate tetrahydrate (99%), dimethyl sulfoxide (99.9%), ethanol (99.5%), toluene (99.8%) and chlorobenzene (99.8%) were purchased from Sigma–Aldrich. TCTA (99.9%) was purchased from OSM. MoO_x (99.95%) and Al (99.999%) were purchased from TASCOS. All chemicals are used as received.

2.1.1 Synthesis of ZnMgO Nanoparticles

1.0427 g of zinc acetate dihydrate and 0.0536 g of magnesium acetate in 30 mL of dimethyl sulfoxide were mixed in a three-neck round-bottom flask at 30 °C. Then, 1.359 g of tetramethylammonium hydroxide in 10 mL of ethanol was injected dropwise into the prepared solution with strong agitation. The mixture was kept at

30 °C for 2.5 h. The ZMO nanoparticles were sunk down for an hour and the solution was centrifuged at 4000 rpm for 5 min. After the centrifugal process, the product was redispersed in ethanol.

2.1.2 Preparation of Precursors for InP Quantum Dots

0.5 M indium oleate ($\text{In}(\text{OA})_3$), 0.5 M zinc oleate ($\text{Zn}(\text{OA})_2$), 2 M TOPSe, and 2 M TOPS stock solutions were prepared for reaction precursors. To prepare 0.5 M $\text{In}(\text{OA})_3$ stock solution, 20 mmol of $\text{In}(\text{Ac})_3$ and a stoichiometric amount of OA are placed in a flask and degassed at an elevated temperature to obtain a clear solution. The reaction flask was filled with argon, and the concentrations of the precursors were diluted to 0.5 M with the solvent. $\text{Zn}(\text{OA})_2$ solution was prepared in a similar method as $\text{In}(\text{OA})_3$. 2 M TOPSe and TOPS stock solutions were prepared by dissolving 50 mmol of Se and S in 25 mL of TOP.

2.1.3 Synthesis of Red-color InP/ZnSe/ZnS Quantum Dots

For a typical synthesis of InP cores, a mixture of 1.8 mmol of $\text{In}(\text{OA})_3$ and 10 mL of ODE was placed into a flask and degassed at 110 °C, before the flask was filled with argon. 1.5 mmol of $(\text{TMS})_3\text{P}$ diluted with TOP was injected into the flask and the flask was then heated up to 280 °C kept for 30 min. Additional injection of 8 mmol of $\text{In}(\text{OA})_3$ and 4.5 mmol of $(\text{TMS})_3\text{P}$ yielded larger InP cores. For the preparation of InP/ZnSe/ZnS QDs, 100 mg of InP cores, 20 mL of TOA, 0.2 mmol of $\text{Zn}(\text{Ac})_2$, and 5 mmol of $\text{Zn}(\text{OA})_2$ were combined into a reaction flask and degassed under vacuum. 1.8 mmol of TOPSe was injected into the flask, and the temperature was raised to 320 °C. Stepwise injection of 6 mmol of TOPSe promotes the further growth of the

ZnSe shell. The additional ZnS shell was overcoated by adding Zn(OA)₂ and TOPS and reacted for 2 h. The reaction mixture was cooled to room temperature and purified.

2.1.4 Synthesis of Green-color InP/ZnSe/ZnS Quantum Dots

All synthesis for QDs were performed under the argon atmosphere through the Schlenk line technique. For the preparation of InP cores, 1.8 mmol of In(OA)₃ precursor, 2 mmol of Zn(OA)₂, and 15 ml of ODE were loaded into a flask, followed by degassed under vacuum. After the flask was filled with argon, a mixture of 1.3 mmol of P(TMS)₃ and an excess amount of TOP was rapidly injected into the reaction flask. The temperature was raised to 260 °C to promote InP nucleation and maintained for 1 hour before cooled to room temperature. Synthesized InP QDs were purified via precipitation/redispersion method and diluted with toluene for further use. To overcoat ZnSe shell onto InP cores, 100 mg of InP cores was injected to the flask containing 5 mmol of Zn(OA)₂ and 15 ml of TOA. 3 mmol of 2M TOPSe was added to the reaction flask and the temperature was kept to 320 °C. Additional Zn(OA)₂, and TOPSe were added to the flask via stepwise injection and reacted for 2 hours for further growth of ZnSe shell. Dropwise injection of TOPS with an excess amount of Zn(OA)₂ yields the formation of the outermost ZnS shell. Synthesized QDs were purified repeatedly via the precipitation/redispersion method.

2.1.5 Surface Ligand Modification of Quantum Dots

The as-synthesized InP/ZnSe/ZnS QDs were precipitated by adding ethanol, followed by redispersion in chlorobenzene (2 mL). After that, hexylamine (1 mL) was added to replace the oleic acid ligands. After 24 h of mixing, the QDs were

precipitated again by adding ethanol to remove residual impurities. The modified QDs were finally dispersed in chlorobenzene.

2.2 Device Fabrication

Glass substrates with pre-patterned ITO electrodes were cleaned with isopropyl alcohol, acetone, and distilled water in an ultrasonic bath for 15 min each. On top of the substrate, ZMO nanoparticles dispersed in ethanol (20 mg/mL) were spin-coated at 2000 rpm for 40 s, and the films were dried under a nitrogen atmosphere at 100 °C for 30 min. Dispersion of QDs in toluene was spin-coated at 4000 rpm for 30 s. PMMA dissolved in acetone (1 mg/mL) was spin-coated at 4000 rpm for 30 sec, resulting in a thickness of 10 nm. Finally, TCTA (50 nm), MoO_x (10 nm), and Al (130 nm) were consecutively deposited using a thermal evaporator.

2.3 Device Characterization

2.3.1 Current-Voltage-Luminance Measurement of QLEDs

The current-voltage (I-V) characteristics were measured with a Keithley 236 source measurement unit, while the electroluminescence was measured with a calibrated Si photodiode (Hamamatsu, S5227-1010BQ) with a size of 10 mm × 10 mm placed at an angle normal to the device surface, assuming that the device was a Lambertian source. To detect a turn-on voltage of light-emitting diodes, we use an ARC PD438 photomultiplier tube (PMT) with the Keithley 236 source measurement unit. The electroluminescence (EL) spectra and the Commission Internationale de L'Eclairage (CIE) color coordinates were measured with a Konica-Minolta CS-1000A spectroradiometer. The luminance and efficiency were calculated from the photocurrent signal of photodiode with a Keithley 2000 multimeter and corrected precisely with the luminance from spectroradiometer (CS-2000).

The chromatic characteristics were calculated from EL spectra measured by the CS-1000A spectrometer using the CIE 1931 color expression system. The tristimulus values XYZ can be calculated by following equations,

$$X = K_m \int_0^{\infty} \bar{x}(\lambda)P(\lambda)d\lambda \quad (2.1)$$

$$Y = K_m \int_0^{\infty} \bar{y}(\lambda)P(\lambda)d\lambda \quad (2.2)$$

$$Z = K_m \int_0^{\infty} \bar{z}(\lambda)P(\lambda)d\lambda \quad (2.3)$$

where, $P(\lambda)$ is a given spectral power distribution of emissive source, \bar{x} , \bar{y} and \bar{z} are the CIE standard color matching functions (see figure 2.1) and K_m is the weighing constant (683 lm W^{-1}). From the tristimulus values, the CIE color coordinates were calculated by following equations,

$$x = \frac{X}{X+Y+Z} \quad (2.4)$$

$$y = \frac{Y}{X+Y+Z} \quad (2.5)$$

$$z = \frac{Z}{X+Y+Z} \quad (2.6)$$

Any color can be plotted on the CIE chromaticity diagram.

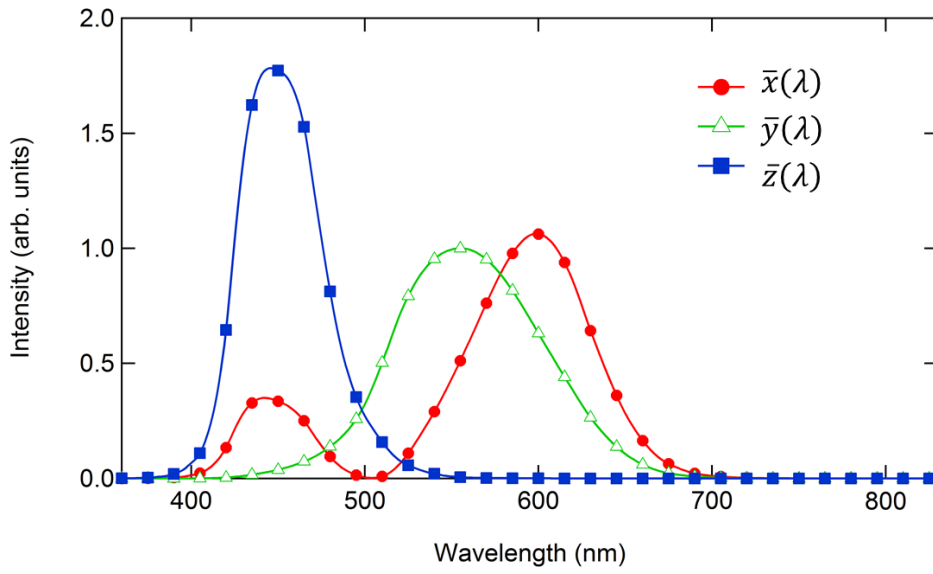


Figure 2.1 The CIE standard observer color matching functions

2.3.2 Efficiency Calculation Methods

To evaluate the emission properties of light-emitting diodes, the commonly employed efficiencies are the EQE, the current efficiency (C.E.) and the power efficiency (P.E.).

The external quantum efficiency can be defined by the following equation.

$$\text{EQE} = \frac{\text{number of emitted photons}}{\text{number of injected electrons}} (\%)$$

Typically, QLEDs or OLEDs emit light into the half plane due to the metal contact. Without any modification for increasing out-coupling efficiency, over 80% of the emission can be lost to internal absorption and wave-guiding in a simple planar light-emitting device.

Since human eye has different spectral sensitivity in visible area, the response of the eye is standardized by the CIE in 1924 (see \bar{y} in figure 2.1). The luminous efficiency weighs all emitted photons according to the photopic response of human eye. The difference is that EQE. weighs all emitted photons equally. C.E. can be expressed by the following equation.

$$\text{C. E.} = \frac{\text{luminance}}{\text{current density}} (\text{cd A}^{-1})$$

The luminance value (cd m^{-2}) can be easily measured by the commercial luminance meter (CS-1000A in this thesis).

The power efficiency is the ratio of the lumen output to the input electrical power as follows,

$$\text{P. E.} = \frac{\text{luminous flux}}{\text{electrical power}} (\text{lm W}^{-1})$$

The EQEs can be useful to understand the fundamental physics for light emission mechanism, while the PEs can be useful to interpret the power dissipated in a light-emitting device when used in a display application.

2.3.3 Operation Lifetime

The operational lifetime was recorded using a McScience M3600 lifetime test system with constant current bias.

2.4 Other Characterization Methods

2.4.1 UV-Visible Absorption

UV-Visible Spectroscopy: The absorption spectra were measured with Agilent Cary 5000 UV-vis-NIR spectrometer. In case of solution, materials were dissolved in toluene or chlorobenzene. For the film measurement, materials were spin-coated or evaporated thermally in the thickness of ~50 nm on quartz substrate

2.4.2 Photoluminescence

PL spectra of QDs were measured Hamamatsu C11119-04 spectrograph pumping samples with a 375-nm laser source in an ambient condition.

2.4.3 Time-Resolved Photoluminescence

The measurements of time-resolved photoluminescence conducted with time-correlated single photon counting (TCSPC) system from Hamamatsu Photonics. All of the time-resolved photoluminescence (TRPL) was measured by 375 nm laser pulse with 1 MHz repetition rate. Trigger delay was adjusted by delay generator.

2.4.4 Transmission Electron Microscopy

The TEM images of the QDs were obtained using FEI Tecnai-F20, and JEOL Ltd JEM-ARM200F Cs-corrected TEM. Samples were treated with Helios 650 focused ion beam for cross-section image.

2.4.5 Scanning Electron Microscopy

Scanning electron microscope (SEM) images were attained with a HITACHI S-5000. Samples were pre-treated by Pt-coating by Ion sputter to mitigate charge-up phenomenon.

2.4.6 Fourier Transform Infrared Spectroscopy

The FT-IR data were obtained with a Bruker Tensor 27 spectrometer in powder state.

2.4.7 Atomic Force Microscopy

The AFM images were taken with a Park Systems XE-150 in a non-contact mode.

2.4.8 Ultraviolet Photoelectron Spectroscopy

The UPS spectra were performed using Kratos AXIS-NOVA, employing He I light source and a hemispherical analyzer. The valence band maximum (VBM) of the nanocrystals was calculated using the following equation.

$$VBM = 21.2 \text{ eV} - |E_{cutoff} - E_{onset}| \quad (2.8)$$

The conduction band minimum (CBM) value was obtained by using the VBM and the excitonic band gaps of QDs, estimated from the PL spectra of QDs.

2.4.9 Thermo Gravimetric Analysis

Thermo gravimetric analysis were conducted using TA Instrument Discovery TGA. The temperature increase rate was 10 °C per minute, and temperature range was from room temperature to 500 °C. The samples was prepared in the form of powder.

Chapter 3

Analysis on operational degradation of InP based QLED

As the growth of the demand for next generation optoelectronics material which has outstanding optical characteristics, quantum dots (QDs) attract attention for the one of the candidates. QDs, inorganic semiconductor nanoparticles, have excellent color purity and high photoluminescence (PL) quantum yield which make it attractive material for display application. Due to the advantageous characteristics for the optoelectronics application, many researches with environmentally friendly materials that do not contain heavy metals and its devices are in progress. As the performance of heavy metal-free QDs is enhanced, understanding of degradation mechanism while operation is become crucial issue for stable device fabrication. Despite the numerous reports about improvement efficiency of heavy metal-free quantum dot light-emitting diodes (QLEDs), the mechanism of luminance deterioration is still insufficiently elucidated. Furthermore, it is difficult to separate the effects of various degradation factors on device during operation as those occurs simultaneously in early deterioration. Because of the multilayer structure of device, charge carriers show the distinct characteristics on each layer. Hence, disparate method ought to be used to

solve each problem, and for this, analyzing the individual degradation component is inevitable process for under stable device fabrication.

In this work, we investigate the effect of excess carriers on degradation of InP-based QLEDs by introducing a charge-imbalanced device structure that is intentionally designed to directly observe how excess holes and electrons influence the QLED lifetime. Also, we analyzed the operational lifetime by dividing it into two components, i.e., temporary and permanent degradation which can be quickly recovered by reverse bias or not, respectively. Interestingly, the hole-excess device exhibited significant permanent degradation with little temporary luminance drop, whereas the electron-excess device showed the exact opposite degradation. In parallel, the PL decay time of QDs upon electrical stress was measured to identify the formation of non-radiative recombination sites. From the results, we infer that excess holes severely affect the formation of defect sites causing non-radiative recombination, leading to permanent degradation of QLEDs. In this experiment, we revealed the effect of each excess carrier on the initial device degradation using optical and electrical methods.

3.1 Characteristics of QLEDs under excess carrier state

For the InP-based QD emissive layer (EML), we synthesized InP/ZnSe/ZnS QDs in a method described in Experimental section, of which properties in terms of absorption and PL spectra, and a TEM image are shown in figure 3.1. As the pristine QLED device, we fabricated an inverted QLED consisting of indium-tin-oxide (ITO, 150 nm)/ZnMgO (ZMO, 40 nm)/QDs (15 nm)/4,4',4"-tris(carbazol-9-yl)triphenylamine (TCTA, 50 nm)/MoO_x (10 nm)/Al (130 nm), as shown in figure 3.2.

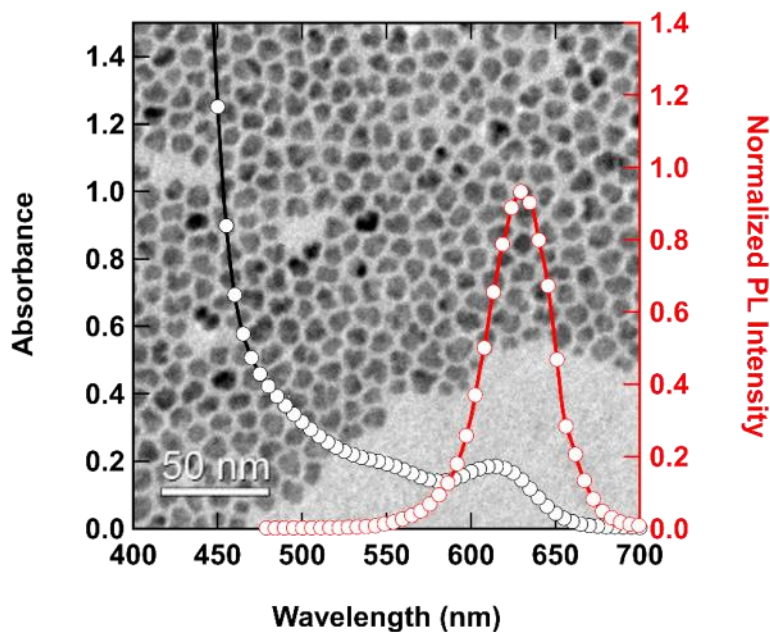


Figure 3.1 Absorption and normalized PL spectra with a TEM image of InP/ZnSe/ZnS QDs.

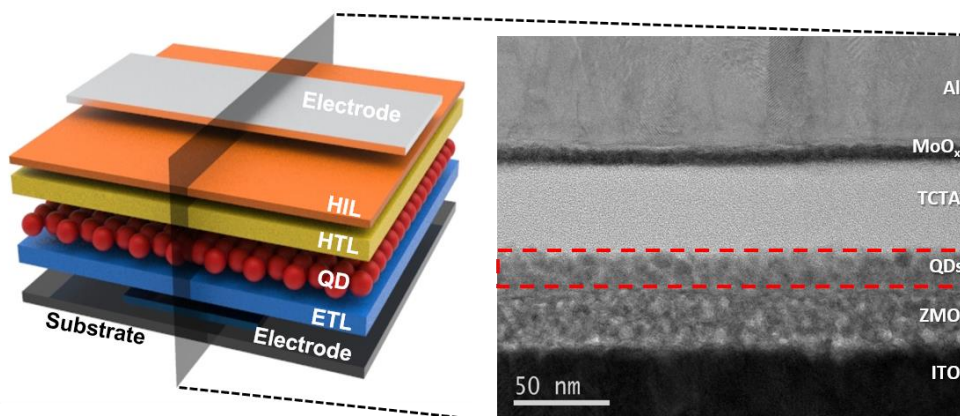


Figure 3.2 Schematic illustration of inverted QLEDs with a cross-section TEM image.

Three types of QLEDs with different carrier injection conditions into the QDs, i.e., the charge-balanced pristine device, hole-excess device, and electron-excess device, were designed as shown in figure 3.3(a)–(c), respectively, with inserting a thin poly(methyl methacrylate) (PMMA) layer (10 nm) between the ZMO and QD layers (resulting in hole-excess) or between the QD and TCTA layers (resulting in electron-excess).

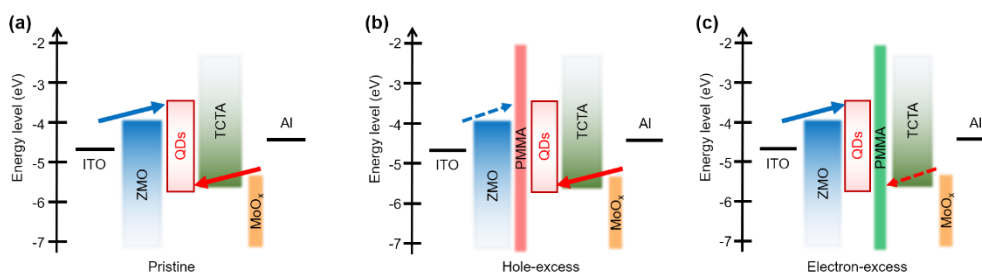


Figure 3.3 Schematic energy diagram of the (a) pristine, (b) hole-excess, and (c) electron-excess devices.

Retarded charge injection and transport by PMMA were also confirmed with a hole-only device (HOD) and an electron-only device (EOD), as shown in figure 3.4. As shown in figure 3.5(a), both current density (J) and luminance (L) at a certain voltage (V) of the hole-excess and electron-excess devices are decreased compared to those of the pristine device because of the insulating PMMA layer. Also, the charge-imbalanced devices exhibited lower current efficiency than that of the pristine device over the entire J regime, as shown in figure 3.5(b). The operational lifetime was measured at a constant current bias of 51 mA/cm^2 where the initial luminance (L_0) was 1820, 1280, and 1090 cd/m^2 for the pristine, hole-excess, and electron-excess devices, respectively. As plotted in figure 3.5(c), the luminance decay at an early stage ($<1 \text{ h}$) is larger in the devices with an insulating layer than the pristine device. However, the electron-excess device shows a stable operation after 1 h, even more than the pristine one. Based on this unexpected phenomenon, we hypothesized that (i) the type of excess carriers affects degradation of QLEDs in different ways, and (ii) the degradation mechanism varies depending on the time-frame. No noticeable change in their electroluminescence (EL) spectra was observed, as displayed in figure 3.5(d).

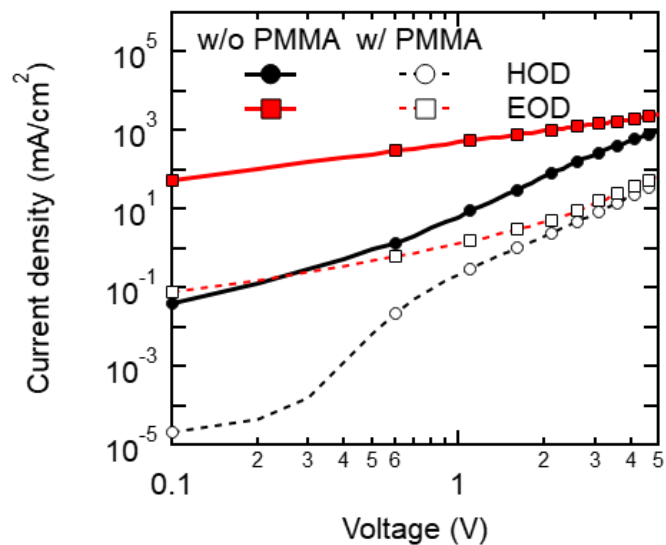


Figure 3.4 J–V characteristics of single carrier devices without and with a PMMA layer. The structure of the HOD is ITO/MoOx (10 nm)/PMMA (0 or 10 nm)/TCTA (50 nm)/MoOx (10 nm)/Al, and that of the EOD is ITO/ZMO (40 nm)/PMMA (0 or 10 nm)/Al.

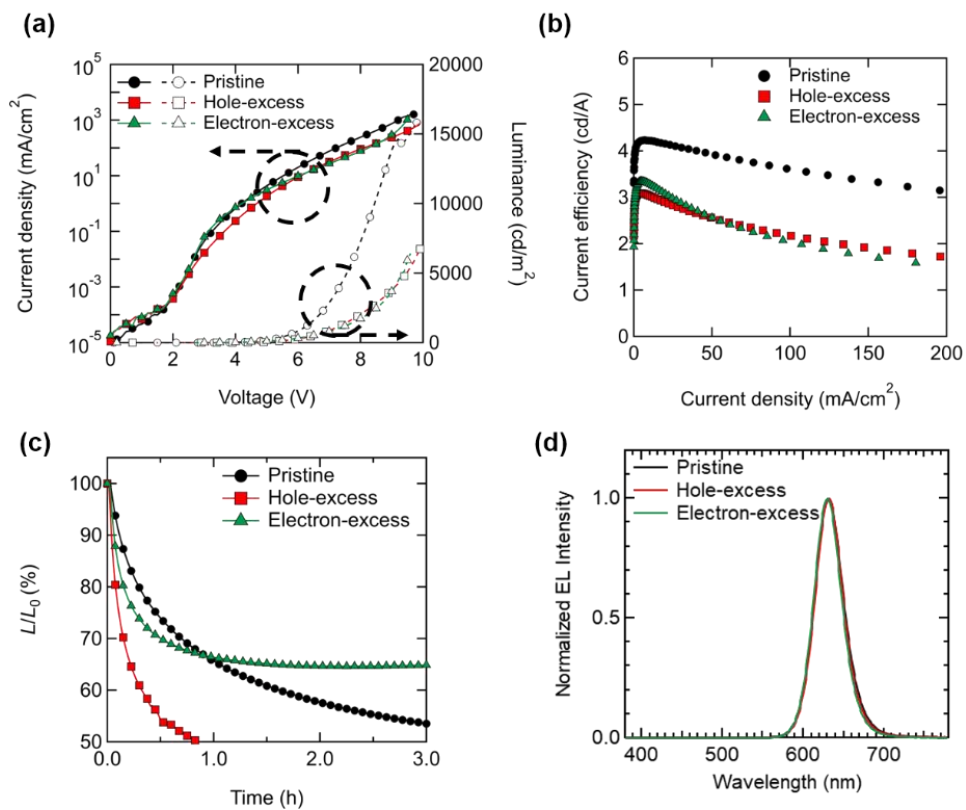


Figure 3.5 Devices characteristics in terms of (a) J–V–L, (b) current efficiency, (c) operational lifetime, and (d) EL spectra.

3.2 Degradation analysis depending on type of luminance drop

Previously, it was reported that early-stage rapid degradation is mainly attributed to the electron-charging effect of Cd-based QDs, and thus it can be recovered by discharging. [23–25] To understand the degradation in InP-based QLEDs depending on excess carriers, we measured the relative luminance change (L/L_0) for an hour with fully discharging the devices every 15 min by applying a reverse bias (-4 V, 15 min) and then cooling down it for additional 30 min with no external bias. As shown in figure 3.6(a), the pristine device showed a typical exponential degradation curve with a slight recovery of luminance soon after the discharging process. Meanwhile, the hole-excess and electron-excess devices show clearly distinctive luminance decay curves. Specifically, the hole-excess device shows a rapid luminance drop with little restoration, and then degraded to below 50% of the initial luminance after about an hour (Figure 3.6(b)). On the other hand, the electron-excess device exhibits a luminance decay, which recovers to over 90% of the initial luminance by discharging (Figure 3.6(c)). Hereafter, we thus defined two different types of degradation, which are irreversible and reversible, as permanent and temporary degradation, respectively. In other words, the hole-excess device suffers permanent degradation, whereas the temporary degradation mechanism is dominant in the electron-excess device. Such a difference of degradation is considered to originate from the type of excess carriers. From the results shown in figure 3.6(a)–(c), we calculated and plotted how much of permanent and temporary degradation present in each device in figure 3.6(d) and 3.6(e). The permanent degradation change is obtained from the difference between the initial relative luminance in each time-frame (see inset of figure 3.6(d)), just after sufficient discharging to exclude reversible degradation. Contrary to this, the

temporary degradation change is defined as the amount restored by discharging in each cycle (see inset of figure 3.6(e)), which is attributed to the luminance decay from a temporary charging effect. From these two graphs, we can again verify that the permanent degradation of InP-based QLEDs is highly affected by excess holes, whereas the electron-excess device experiences much smaller permanent degradation than the others and even hardly shows further degradation after 30 min. We thus assume that excess holes cause fatal failures at the surface of QDs and/or at the interfaces of QLEDs. An additionally noticeable point is that over two thirds of the total permanent degradation occurs within the first 15 min in all of the devices, presenting that any changes for this degradation are created in a quite short time. Meanwhile, the temporary degradation is dominant in the electron-excess device (16.7 percentage-point in average) but not in the pristine (3.9 percentage-point in average) and hole-excess devices (2.7 percentage-point in average), meaning that electron charging disturbs radiative recombination principally but temporarily. Because the amount of the temporary degradation in each cycle is almost identical, charging and discharging in InP QDs are considered to be reversible and repeatable. Overall, we can infer that the major constituent of early-stage degradation in the charge-balanced (i.e., pristine) InP QLED is the irreversible permanent degradation rather than the reversible electron charging.

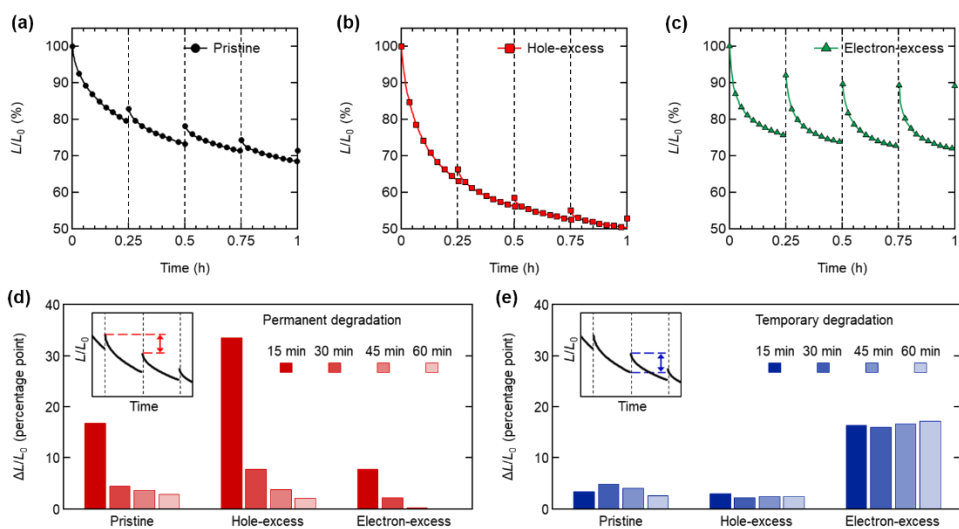


Figure 3.6 Operational lifetime of the (a) pristine, (b) hole-excess, and (c) electron-excess devices with discharging every 15 min. The difference of the (d) permanent and (e) temporary degradation in each cycle. The inset image shows how to obtain the values.

3.3 Origin of temporary degradation

First, in order to analyze the cause of strong temporary deterioration of electron excess devices, TRPL was measured during device operation as shown in figure 3.7. When measuring transient PL while driving a device, a steady EL signal and a PL signal by a transient pulse are simultaneously measured. At this time, the exciton decay time during driving can be known by excluding the constant EL signal from the entire range before the pulse. It was found that the exciton lifetime of the electron excess device before and after operation was the same, but during operation, the lifetime was significantly reduced. It can be seen that non-radiative auger recombination increased due to an excess of electrons in the QD. A device with an average exciton lifetime of 12.3 ns before operation has a relatively short exciton lifetime of 6.8 ns during operation. The following exciton lifetime decrease is considered to be the main cause of luminance decrease during operation.

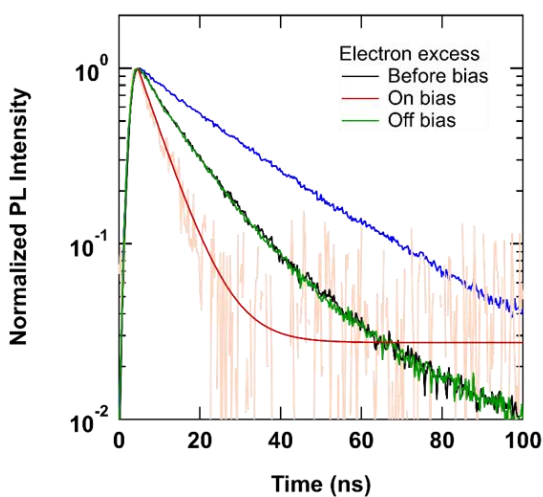


Figure 3.7 TRPL curve of device (blue line: TRPL of QD in solution state)

As another factors, there is joule heat that inducing temporary change of carrier transportation or permanent material degradation. Figure 3.8 shows the temperature of devices during operation by thermal camera with same initial condition. We observed the temperature in light emitting region of the devices increase with the lapse of driving time and it saturated after few minutes. Although the temperature difference between before operation and after saturation is strong in the control devices with high current density, the amount of temperature change is not enough to significantly affect the mobility of the transport layer and does not rise above the transition temperature of the materials that used. In addition, film roughness of ZnO/QD, ZnO/PMMA/QD and ZnO/QD/PMMA have similar value shown in figure 3.9. Consequently, main cause of temporary luminance degradation is considered the charging effect on QDs.

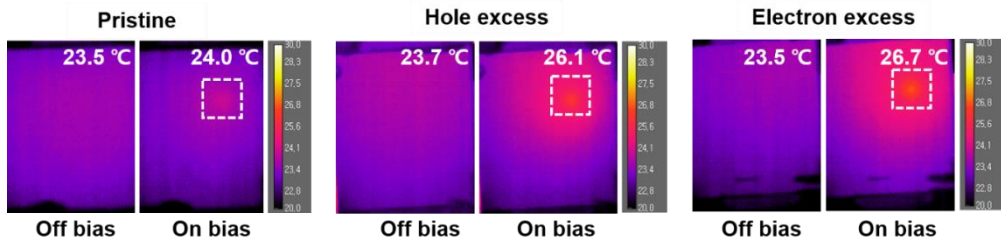


Figure 3.8 Temperature change during electrical operation of (a) pristine (b) hole excess (c) electron excess devices

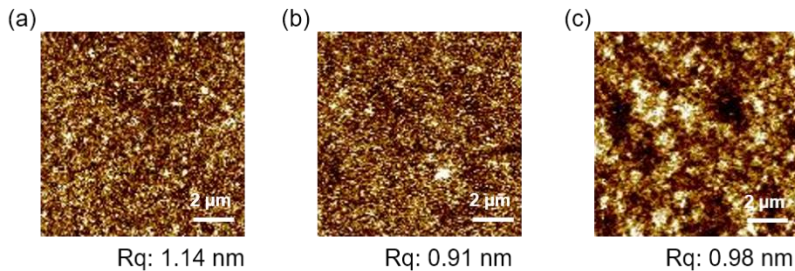


Figure 3.9 AFM image of (a) ZnO/QD, (b) ZnO/PMMA/QD, (c) ZnO/QD/PMMA

3.4 Origin of permanent degradation

To further identify the cause of different degradation in the InP-based QLEDs, we first measured the PL decay time constant (τ_{PL}) of the QD layer in the full device with TRPL technique at 15-min intervals upon current bias, as shown in figure 3.10(a)–(c). To avoid any conceivable interaction of excitons with charged electrons in QDs and/or localized charges adjacent to the QD layer, [28,43] we discharged the devices in the same way as mentioned above before the TRPL measurement. In the pristine device, the τ_{PL} was decreased by 22.7%, from 12.22 ns to 9.45 ns, mainly after the first 15 min of operation, and then gradually saturated to 8.34 ns until 60 min (see figure 3.10(a) and Table 3.1. By comparison, the charge-unbalance devices exhibit distinguishing PL decay characteristics depending on the type of excess charges. In the hole-excess device, much larger decrease of τ_{PL} was observed at the first time-frame, from 11.94 ns to 8.06 ns (by 32.5%). On the other hand, the QD layer in the electron-excess device barely shows perceptible τ_{PL} change even after 60 min of bias stress. These results and trends are analogous to the permanent degradation difference at each interval plotted in figure 3.6(d), implying that excess holes cause unrecoverable damage to the surface of QDs, for instance, detachment of electrochemically unstable ligands. [31] To reconfirm the results, we conducted the same experiment with single-carrier devices in which any effects of counter charges can be eliminated. As shown in figure 3.10(d) and (e), an EOD [ITO/ZMO (40 nm)/QD (15 nm)/ZMO (40 nm)/Al] and a HOD [ITO/MoO_x (10 nm)/QD (15 nm)/TCTA (50 nm)/MoO_x (10 nm)/Al] were fabricated, electrically stressed at a constant current bias ($J = 5.1 \text{ mA/cm}^2$), and their TRPL signals were measured every 15 min. Similar to the results in the full devices, the EOD exhibits no noticeable change of τ_{PL} for 30 min, while the HOD shows conspicuous decrease of τ_{PL} , from

11.15 ns to 8.37 ns, at the first interval. To surely exclude the effect of hole-carriers potentially piled up at the QD/TCTA interface during operation, we measured the TRPL of another HOD with a 10-nm PMMA spacer layer in between, as shown in figure 3.10(f). The τ_{PL} values were slightly increased due to the PMMA layer but the reduced τ_{PL} (from 11.98 ns to 9.76 ns) only in 15 min is sufficient to verify the early-stage permanent degradation of QDs by excess holes. Consequently, excessive hole injection is considered the most significant reason for the early-stage permanent degradation of InP-based QLEDs, originating from rapid formation of surface defects in QDs.

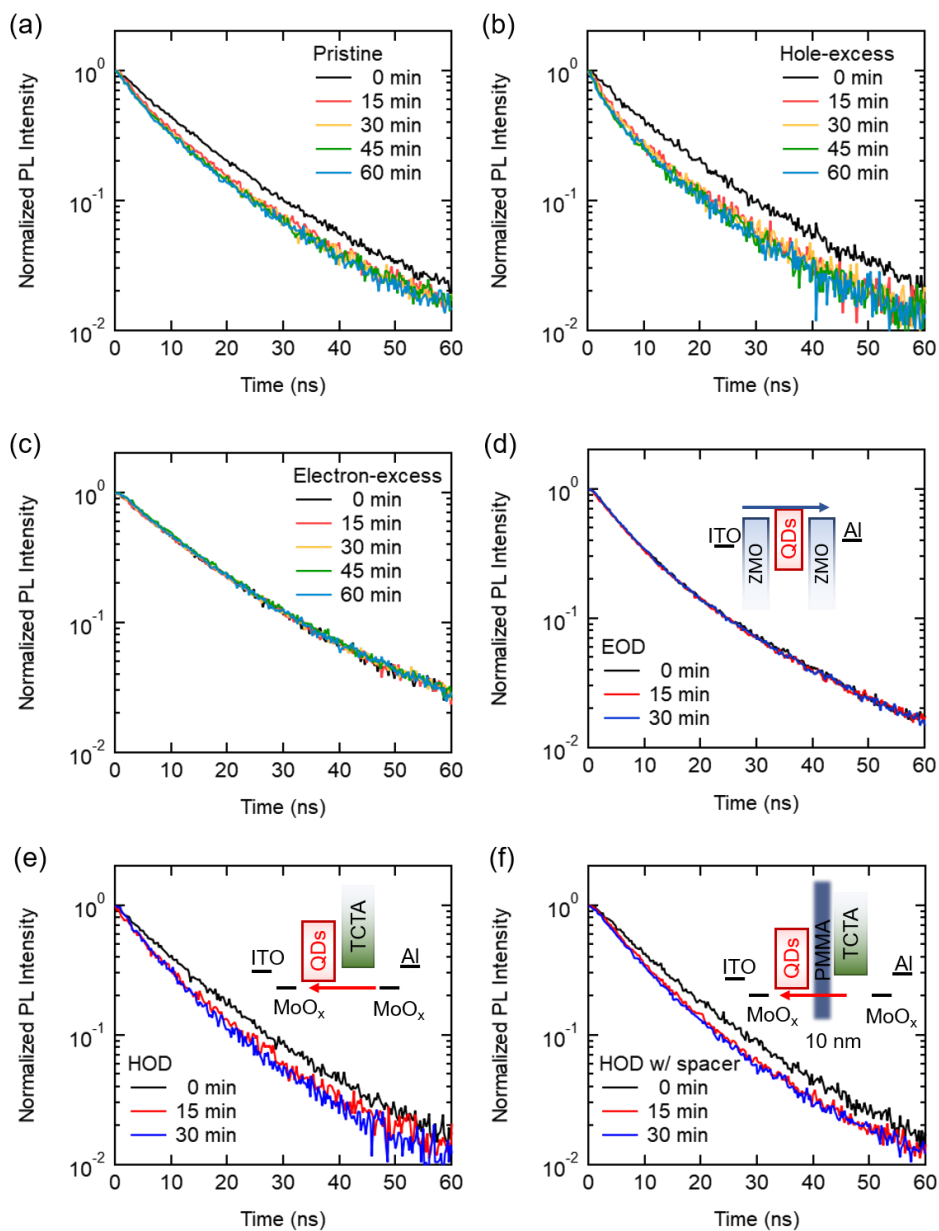


Figure 3.10 TRPL decay curves of the (a) pristine, (b) hole-excess, and (c) electron-excess QLEDs, and the (d) EOD, (e) HOD, and (f) HOD with a PMMA spacer layer, measured at 15-min intervals.

Table 3.1 TRPL decay time in QLEDs and single-carrier devices.

Device	TRPL decay time constant ¹⁾ (ns)				
	0 min	15 min	30 min	45 min	60 min
Pristine	12.22	9.45	9.17	8.62	8.34
Hole excess	11.94	8.06	7.51	6.80	6.39
Electron excess	12.77	13.05	13.05	13.03	13.13
EOD	9.19	-	8.91	-	8.91
HOD	11.15	-	8.37	-	7.81
HOD w/ PMMA	11.98	-	9.76	-	9.20

¹⁾The decay time corresponding to $1/e$ of the initial intensity.

In addition, we measured the J–V characteristics of two different type of HODs, with and without QDs layer, to confirm the formation of surface defect site. Degradation was conducted with constant current bias ($J = 5.1 \text{ mA/cm}^2$) for 15 minutes. As shown in figure 3.11, J–V characteristics of HOD w/o QDs rarely changed after constant current operation. In contrast, current density is much decreased in range of 0.1–4 V at HOD with QDs layer after degradation. Furthermore, the trap filled limit voltage point increased to about 0.8 V to 1.6 V after deterioration. The following results can be indicators of an increase in trap density in the device during degradation. [43–45] Therefore, it is expected that defect sites were formed on surface of QDs along with the decrease in PL decay time.

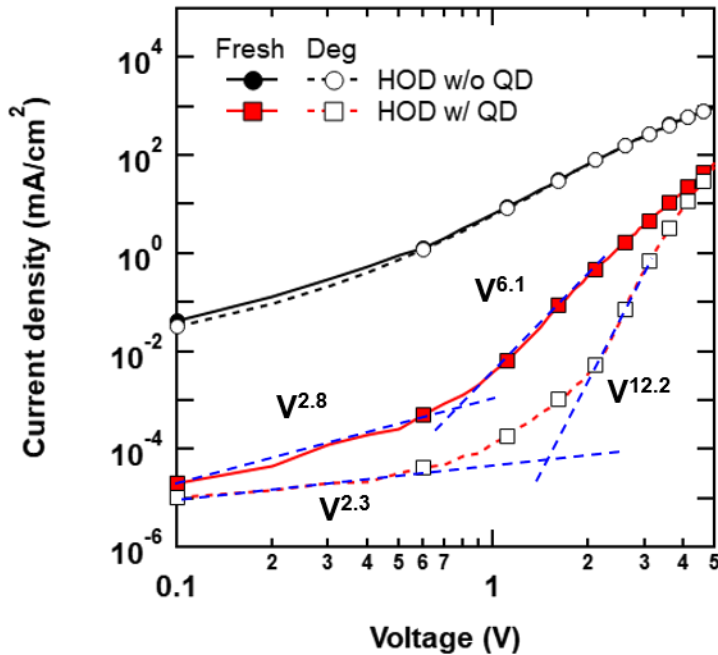


Figure 3.11 J–V characteristics of HOD before and after degradation.

3.5 Summary

In summary, we investigated factors affecting the stability of InP-based QLEDs by purposely design the device to make one type of carriers (i.e., holes or electrons) dominate during electrical operation. From the lifetime measurement with discharging the QLEDs at regular intervals, we could divide the amount of degradation into permanent and temporary degradation which are unrecoverable and recoverable, respectively. Temporary luminance drop tends to occur with excess electron state on QDs and decreased PL decay time is recovered after discharging process. Contrary, we found that the permanent degradation occurs because excess holes rapidly degrades the QDs, which is confirmed by TRPL experiments in the charge-imbalanced QLEDs and single-carrier devices. We expected our research can contribute the development of stable InP-based QLEDs.

Chapter 4

Stability enhancement of QLED via ligand exchange method

As the one of the elements constituting the QDs, surface ligands can greatly influence the characteristics of the QDs. During synthesis process of QDs, various ligands are used to control growth and enable QDs to be maintained in a colloidal state in a solvent. [46–49] In addition, surface passivated ligand can effectively decrease generation of surface defect by hindering oxidization of QDs and ligand also used to remove additional defect sites created after synthesis. [50–52] Surface ligands have great influence not only stability and synthesis control, but also the surface energy of the QDs which is affecting electrical characteristics. [53–57] Therefore, various characteristics can be obtained through the combination of numerous types of QDs and ligands, which suggests that desired feature can be derived within the application only by ligand substitution.

In this work, we investigated characteristics of InP/ZnSe/ZnS QDs with oleic acid and hexyl amine ligand. In the previous chapter, deterioration of QDs is accelerated in a state where holes are dominant which is origin of permanent luminance drop during operation. As the cause of degradation, we suspected ligand

dissociation by holes because the oleate surface capping ligand can accept electron or hole causing dissociation of ligand from surface. [58,59] Generation of unpassivated surface sites effectively lower PLQY of QDs and act as carrier trap site that lowers the stability of the device. [60,61] To verify the assumption, we applied an alkyl amine ligand known to be relatively strong and stable through a ligand substitution method. [31] First, we confirmed that the ligand substitution occurred properly, and then analyzed the characteristics of QDs. In addition, we clarify stability of device can be improved through ligand substitution by analyzing the effect of the change of ligand-substituted QDs on device.

4.1 Ligand exchange of InP/ZnSe/ZnS QDs.

To exchange surface ligand of InP/ZnSe/ZnS QDs, we used thermodynamic ligand exchange method. [62] As the ligand displacement process depends on a number of factors such as particle size, ligand length and binding energy of anchoring group. Thus, we used hexylamine, which is short in length, which is advantageous for ligand substitution. FT-IR was measured to confirm the ligand substitution as shown in figure 4.1. After ligand exchange process, stretching vibration peak of N-H appears at 3500–3150 cm^{-1} . The result suggests the presence of alkyl amine on the surface of QDs. However, FT-IR spectrum also show the COO^- signals around 1540 and 1420 cm^{-1} are still obvious after the ligand displacement process. It can be understood that the both ligand, oleic acid and hexylamine, are coexist because ligand exchange of as-synthesized QDs is partially occurred. [63,64]

We conducted thermogravimetric analysis for prediction of ligand substitution ratio. Before the ligand exchanged process, QDs show the 10.7% decreased which is attributed by sublimation of zinc oleate ligand as shown in figure 4.2. After ligand exchanged process, the portion of solid residue of QDs was increased and the amount of decrease ratio is about 5.3%. As the ZnS-hexylamine compound show weight loss from 140 $^{\circ}\text{C}$ to 400 $^{\circ}\text{C}$ [65], weight loss of 5.3% includes the sublimation of OA and HA both. Consequently, we expect over the half of OA was replaced and ligand substitution rate to be around 60 to 70%

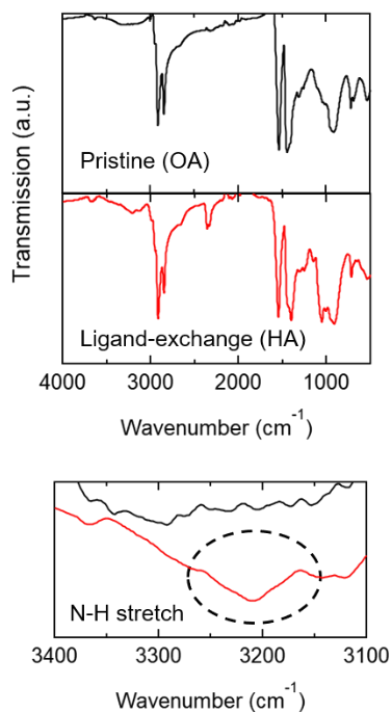


Figure 4.1 FT-IR measurement of oleic acid and hexyl amine ligand QDs

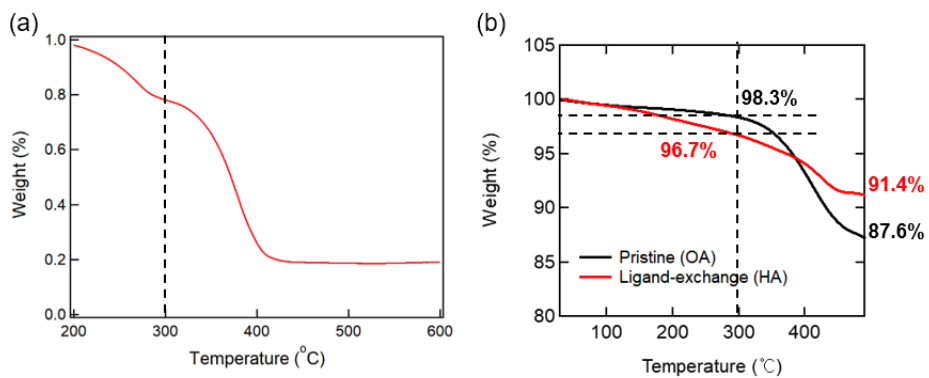


Figure 4.2 TGA result of (a) zinc oleate and (b) QDs with OA and HA ligand

Another evidence of ligand substitution is the energy level shift of QDs. Unlike carboxyl acid, the electron donating ligand or ion, such as amine ligand can shift surface energy level in the cathodic direction. [55] In this experiment, the energy level of ligand exchanged QDs is upshifted by 0.3 eV when measuring the UPS as depicted in figure 4.3 and it has consistency with previous report. [66] Therefore, we expect that ligand substitution process is made and two kinds of ligands are co-existed on QDs surface.

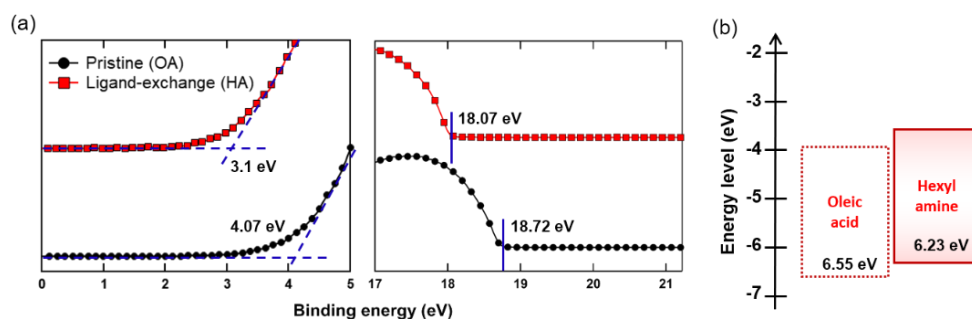


Figure 4.3 Ultraviolet photoelectron spectroscopy and schematic energy diagram of QD

To confirm that ligand substitution affects on optical characteristics, we measured UV-vis and TR PL as shown in figure 4.4. No significant changes in the UV-vis and PL spectra meaning that ligand substitution had no significant effect on core properties. However, τ_{PL} in solution state was slightly decreased, from 26.3 ns with OA to 19.7 ns with HA, due to the defects formed during the solution-based ligand exchange process. [63]

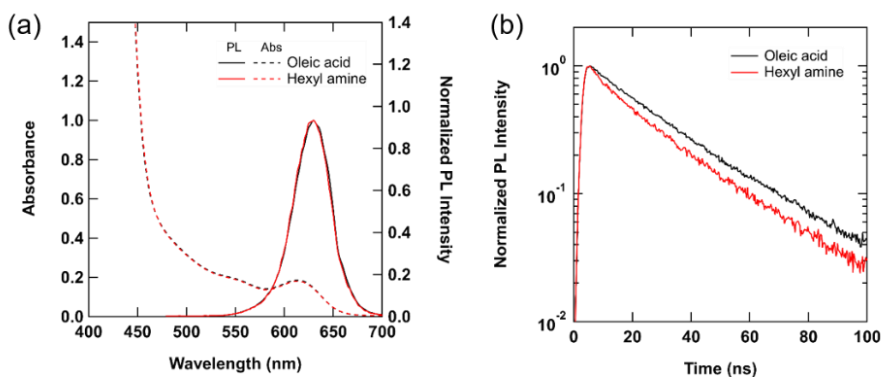


Figure 4.4 (a) Absorbance, PL spectrum and (b) TRPL decay of oleic acid and hexyl amine ligand QDs in solution state

The morphology of the thin film was observed because not only the optical properties but also the roughness of the film can affect the device. figure 4.5 shows the AFM image of the QD film. In oleic acid, root mean square (Rq) which represent the roughness degree has 1.54 nm and hexyl amine ligand has 1.36 nm which It was confirmed that the surface roughness was improved upon ligand substitution, which can reduce the strong voltage applied to the local area. In addition, inset of figure 4.5 show the SEM image of QDs film and there was no significant feature change was observed.

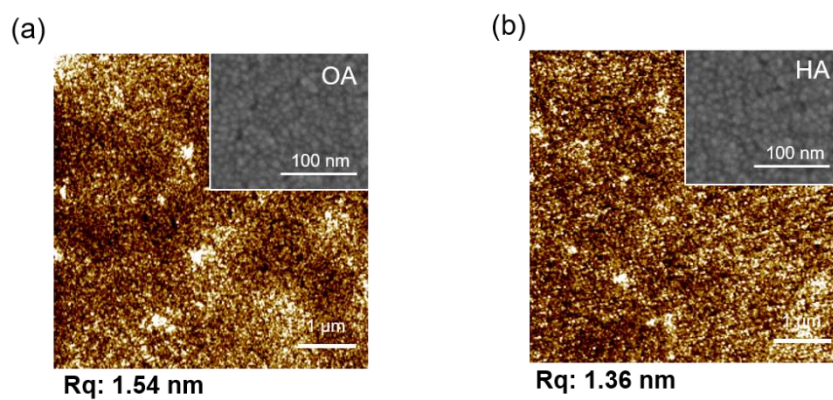


Figure 4.5 AFM image of (a) Oleic acid QD (b) Hexyl amine QD film inset of (a) and (b) represent SEM image of QD film

4.2 Effect of ligand exchange on device characteristics

Figure 4.6 compare the J–V–L, current efficiency, and EL spectra of the QLEDs before and after ligand-exchange. Overall current injection is increased at ligand exchange device and the increase is expected to be due to the energy shift of the QDs. Owing to the amine anchoring group, luminance of the QLED with the HA ligand are also increased (e.g., maximum L: 14650 cd/m² with OA and 36540 cd/m² with HA ligands). The new device shows lower current efficiency at the low J region (<200 mA/cm²) that may be attributed to the unavoidable defects formed during ligand exchange, but the efficiency is higher when J >200 mA/cm² with reduced roll-off. In addition, it was confirmed again that the EL spectrum peak point was 628 nm and the FWHM was 40 nm, indicating ligand exchange process did not significantly affect the spectral wavelength.

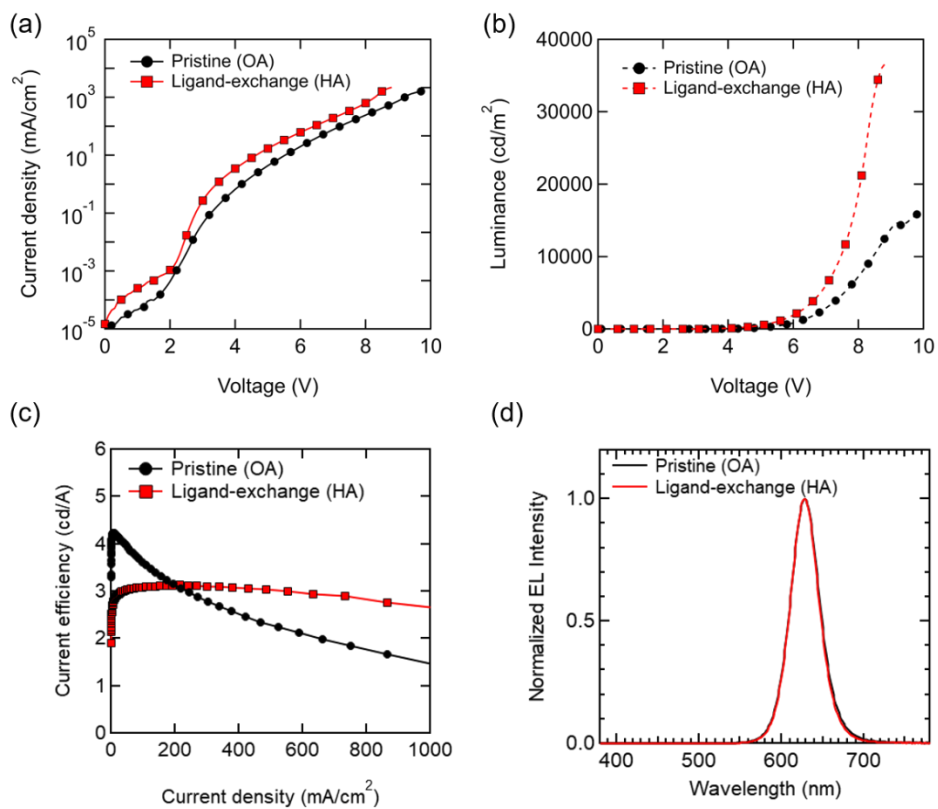


Figure 4.6 Comparison of the performance of QLEDs with OA and HA ligands, in terms of (a) J–V, (b) L–V (c) current efficiency, and (c) EL spectrum

Figure 4.7 (a) shows that the estimated half-lifetime (T50) measured at the constant current bias of 51 mA/cm² was dramatically increased as we expected, from 3.6 h for the QLED with OA ($L_0 = 1820$ cd/m²) to 547 h for the device with HA ($L_0 = 1520$ cd/m²), of which corresponding T50 values with $L_0 = 100$ cd/m² (acceleration factor = 1.8) are 667 h and 72757 h, respectively, over 109-times longer. As shown in figure 4.7(b)–(d), we measured relative luminance change (L/L_0) for an hour with fully discharging the devices every 15 min by applying a reverse bias and then cooling down it for additional 30 min with no external bias for both QLEDs with OA and HA ligands. The pristine QLED shows significant permanent luminance decrease in first 15min cycle and the amount is gradually decrease. Amount of temporary degradation at each cycle was maintained around 5 %. But the device with HA exhibits extremely small permanent degradation through the whole cycle. Although the average of temporary luminance drop is slightly higher than that of Pristine, it can be negligible compared to the permanent luminance reduction difference. Therefore, ligand substitution can effectively improve permanent luminance reduction.

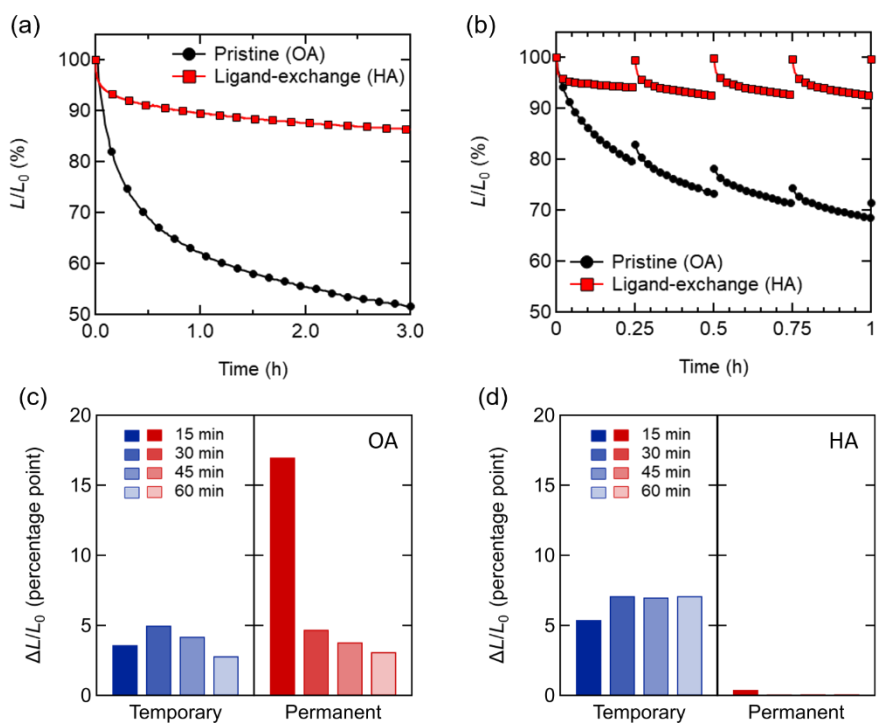


Figure 4.7 (a) Comparison of the performance of QLEDs with OA and HA ligands, in terms of operational lifetime. (b) Relative luminance with discharging and the permanent and temporary degradation at 15-min intervals of (c) OA (d) HA device

To confirm the early-stage permanent decrease in luminance is stem from degradation of QDs, TRPL was measured before and after deterioration as shown in figure 4.8. The exciton decay times of QDs in each device before degradation were 12.22 ns and 10.02 ns, which were relatively longer in oleic acid. This is considered to be due to a surface defect of QD during substitution, as shown in figure 4.4 (b). After 1 hour of deterioration, the decay time decreased significantly to 8.34 ns in the case of oleic acid and there is no change in the case of hexyl amine devices. These results also support the amine ligand exchange can improve the electrical stability of QDs during operation.

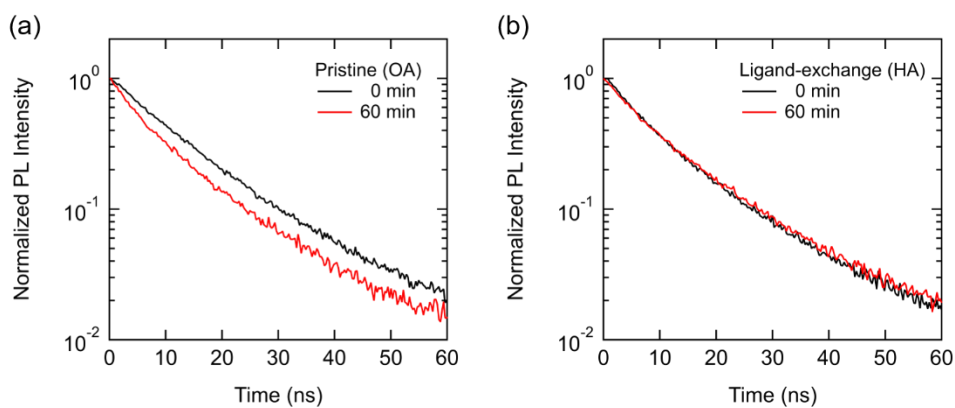


Figure 4.8 TRPL decay of (a) oleic acid ligand QD device and (b) hexyl amine ligand QD device before and after 1 hour degradation

Furthermore, to elaborately examine how surface energy shift of QD have an effect on device electrical properties, we investigated with impedance spectroscopy analysis. Impedance spectroscopy is a useful tool to study interfacial electrical properties such as carrier injection and transportation of devices and has been widely utilized in the field of OLED. Electrical properties of conductivity and resistivity as a function of frequency can be explained according to complex ac impedance, $Z=R - jX$, where R is the real part and X is the imaginary part of impedance. Figure 4.9 represent the Cole-Cole plot of devices during operation time interval. We measured impedance of QLED at bias of 3.5 V, frequency sweep from 100 to 50 MHz with amplitude of 10 meV. Cole-Cole plot shows semicircle for all devices and the diameter of each semicircle can be interpreted as the charge transfer resistance in devices. At 0 min, hexyl amine ligand much lower resistance than Oleic acid and it is result of reduced hole injection barrier. Furthermore, it can be seen that the increase rate until the cole-cole plot is saturated during operation is approximately 21% for oleic acid and 15% for hexyl amine, and it can imply the effect of accumulated space charged is also reduced. Ligand substitution not only enhances the stability of QDs, but also improves operational stress due to energy shift.

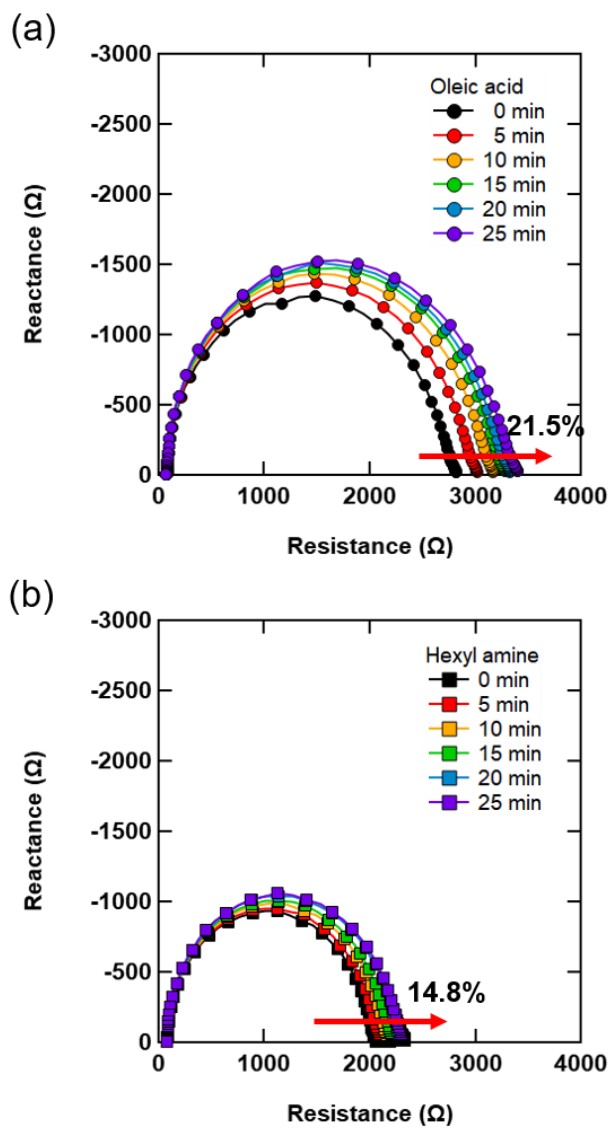


Figure 4.9 Operation time dependent nyquist plot of (a) oleic acid ligand QLED (b) hexyl amine ligand QLED

4.3 Versatility in improving the stability by ligand exchange strategy

In our previous experiment, we confirmed that ligand modification of red-color InP/ZnSe/ZnS QD can effectively enhance the operational stability increasing the lifetime. Therefore, to clarify whether the following method is universally applicable, the strategy applied to green-color InP/ZnSe/ZnS QDs having the same composition with red-color QDs. The ligand substitution method was performed in the same manner as in the previous experiment. As shown in FT-IR measurement in figure 4.10, surface modification QDs exhibiting the N-H stretching peak at $3500\text{--}3150\text{ cm}^{-1}$ with the COO^- signals around 1540 and 1420 cm^{-1} peak. It indicates the both ligand, oleic acid and hexyl amine, are coexist on the surface of QDs which is similar feature with red-color QDs.

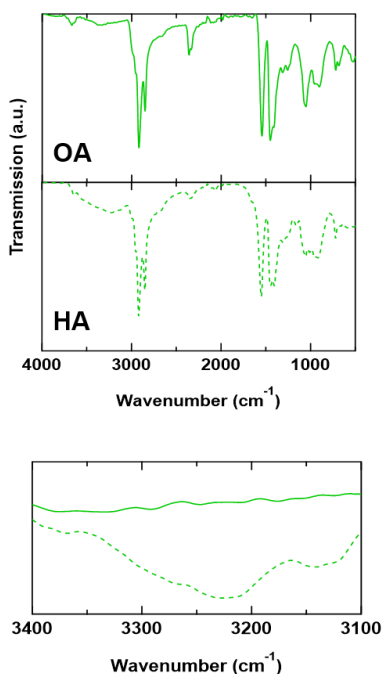


Figure 4.10 (a) FT-IR measurement of green InP QDs

As shown in figure 4.11(a), optical characteristics of QDs, absorption and PL spectrum, are rarely changed after ligand substitution. Since there was almost no change in the QD absorption and PL spectrum measurements in solution, it was confirmed that ligand substitution did not affect the core properties even in green-color QDs. Figure 4.11 (b) shows the exciton lifetime in solution. The average PL decay time of QD with oleic acid is 20.28 ns, whereas that of the ligand modification QD is 14.46 ns. This is also considered to be a surface defect that occurs during the substitution process.

Figure 4.12 (a) shows the UPS result of QD film. It can be seen that the VBM of the QD before ligand substitution is 7.02 eV, whereas the VBM of the QD after the substitution is 6.69 eV, which is about 0.33 eV upshifted. As we mention above, the electron donating ligand or ion, such as amine ligand can shift surface energy level in the cathodic direction. In addition, the amount of energy shift by ligand exchange is similar with that of red-color QDs expecting the exchange ratio also similar. Therefore, the ligand substitution shows the same properties in green InP QDs as red-color QD.

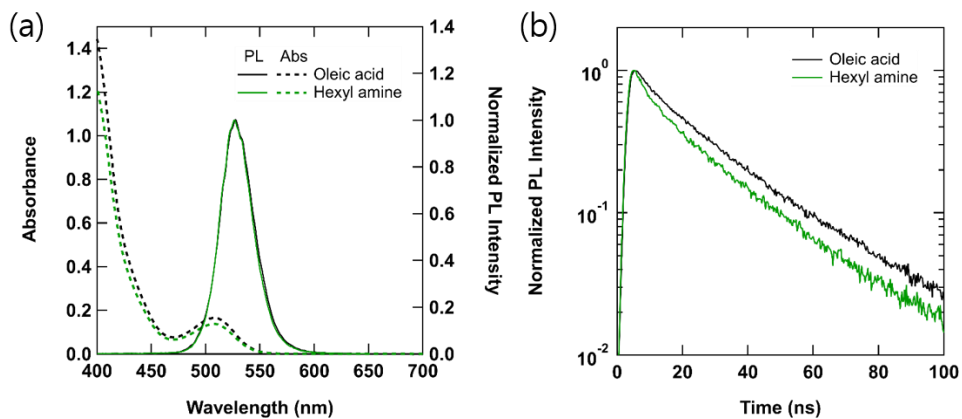


Figure 4.11 (a) Absorbance, PL spectrum and (b) TRPL decay of green oleic acid and hexyl amine ligand QDs in solution state

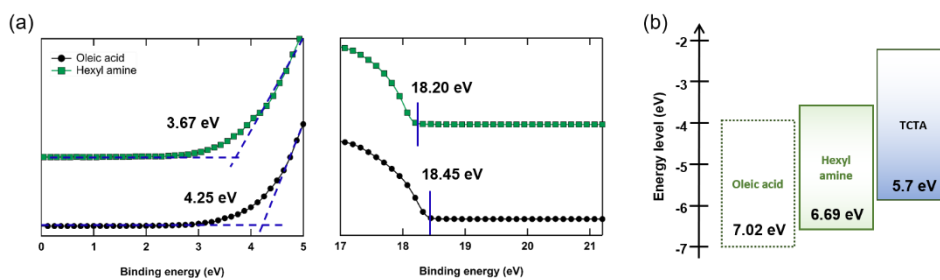


Figure 4.12 (a) UPS measurement of oleic acid and hexyl amine ligand green InP QDs. (b) Schematic energy diagram of QDs and TCTA

Figure 4.13 shows the electrical and optical characteristics and lifetime of the device. Figure 4.13(a) represent the J–V–L curve of the device, and like the red QD, it was possible to observe the increase in current density and luminance in the range of driving voltage. Also, as shown in figure 4.13(b), the highest value of current efficiency decreases from 5.2 cd/A to 4.3 cd/A, but efficiency of QLED with the HA ligand is higher than that of OA ligand when $J > 100 \text{ mA/cm}^2$. Figure 4.13(c) shows the change in luminance with time at a constant current density with 51 mA/cm^2 where the initial luminance (L_0) was 2200 and 1900 cd/m^2 . After ligand exchange, half-lifetime is much enhanced about 56-fold from 0.36 hour of OA to 18.95 hour of HA. Therefore, it was found that surface ligand modification can be universally applied not only to red-color InP/ZnSe/ZnS QD but also to green having the same material composition, and greatly increases the lifespan characteristics of the device. And as there is no change in the EL spectrum in figure 4.13(d), it can be seen that the core characteristics did not change. All the characteristics of the green-color InP QLED are very similar to those shown in the red-color InP QLED device. Thus, ligand substitution method can effectively increase the lifetime of QLEDs and is applicable to InP QDs having other wavelengths.

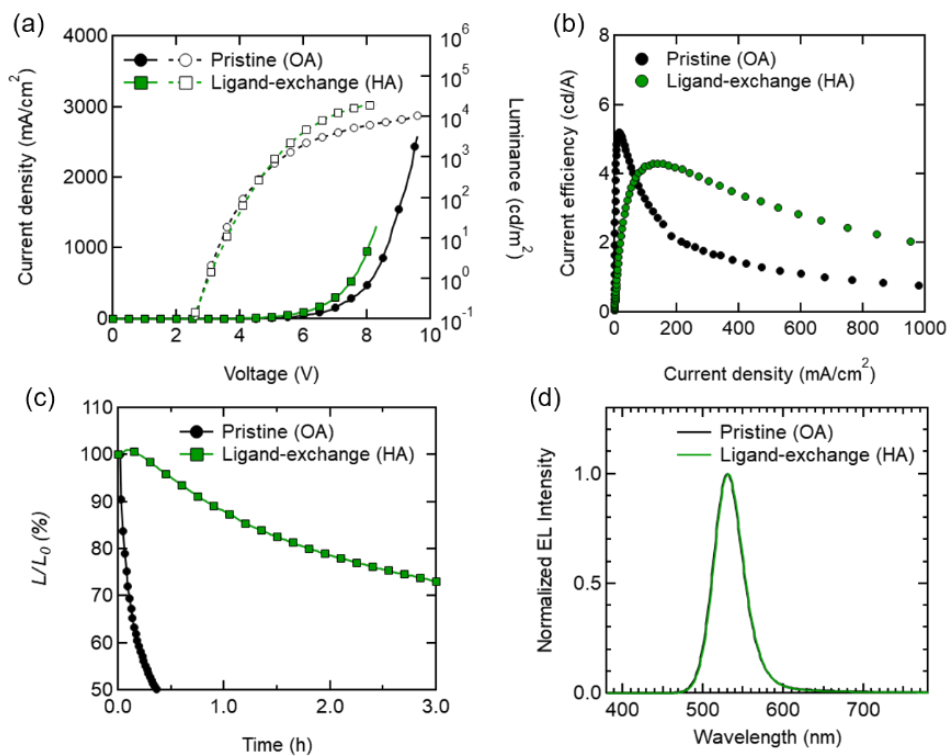


Figure 4.13 Comparison of the performance of green-color InP/ZnSe/ZnS QLEDs with OA and HA ligands, in terms of (a) J–V–L, (b) current efficiency, (c) operational lifetime, and (d) normalized EL spectrum.

4.4 Summary

In this experiment, the amine ligand substitution characteristics of InP-based QDs and their application to LEDs were analyzed. The ligand substitution method did not affect the PL spectrum and absorption exhibited by the core as expected. However, the PL decreased due to degradation of QDs due to the optimization issues of the substitution process. Although the ligand substitution occurred partially on shell, it was sufficient to change the surface state of the QDs. Energy level of the QDs surface was upshifted due to the characteristics of the amine ligand that donates electrons for binding process, which facilitated the injection of holes and reduced the injection of electrons in the devices structure. Especially, the operational stability of the device is greatly increased by effectively suppressing degradation of QDs, one of the causes of deterioration of InP QLEDs, through an electrochemically stable bond than oleic acid. In addition, it was proved that utilization of amine ligand universally increases operational stability of QLED by confirming that the ligand substitution method can be applied not only to red-color QDs but also to green-color QDs with the same composition.

Chapter 5

Conclusion

In this thesis, we analyze and enhance operational stability of InP/ZnSe/ZnS based QLED.

First, we investigated factors affecting the stability of InP-based QLEDs by purposely design the device to make one type of carriers (i.e., holes or electrons) dominate during electrical operation by insertion of insulating layer. From the lifetime measurement with discharging the QLEDs at regular intervals, we could divide the amount of degradation into permanent and temporary degradation which are unrecoverable and recoverable, respectively. Excessive electron state on QDs played a large role in the cause of the temporary operational luminance drop as well known. We found that the permanent degradation occurs because excess holes rapidly degrades the surface of QDs, which is confirmed by TRPL experiments in the charge-imbalanced QLEDs and single-carrier devices. Furthermore, electrical characteristics of hole only devices represent the formation of defect state expected to generated on surface of QDs.

To diminish the permanent cause of deterioration, we introduced an electrochemically stable ligand, hexylamine, for InP-based QDs by the ligand exchange method. Although the ligand substitution method not entirely exchange the

existing ligand, it is sufficient to change the characteristics of QDs. As the ligand substitution occurred at surface of QDs, characteristics of core, PL spectra and absorption, are preserved after ligand exchange. Surface energy of QDs changes in a favorably for electrical operation, improving efficiency roll-off. Especially, ligand exchanged method effectively enhanced stability of device resulting in over 109 times longer lifetime with no noticeable early-stage permanent degradation. In addition, the ligand substitution method proved its versatility by confirming that it could be applied to green-color InP/ZnSe/ZnS QDs.

Conclusively, we therefore believe that our strategies to reveal the effects of excess carriers on the device lifetime and to demonstrate QLEDs with little permanent degradation would be practically applicable for the development of highly stable InP-based QLEDs in following research.

Bibliography

- [1] Chuang, C.-H. M.; Brown, P. R.; Bulović, V.; Bawendi, M. G., Improved performance and stability in quantum dot solar cells through band alignment engineering. *Nature materials* **2014**, *13* (8), 796-801.
- [2] Jaiswal, J. K.; Goldman, E. R.; Mattoussi, H.; Simon, S. M., Use of quantum dots for live cell imaging. *Nature methods* **2004**, *1* (1), 73-78.
- [3] Klimov, V. I.; Ivanov, S. A.; Nanda, J.; Achermann, M.; Bezel, I.; McGuire, J. A.; Piryatinski, A., Single-exciton optical gain in semiconductor nanocrystals. *Nature* **2007**, *447* (7143), 441-446.
- [4] Kozlov, O. V.; Park, Y.-S.; Roh, J.; Fedin, I.; Nakotte, T.; Klimov, V. I., Sub-single-exciton lasing using charged quantum dots coupled to a distributed feedback cavity. *Science* **2019**, *365* (6454), 672-675.
- [5] Lim, J.; Park, Y.-S.; Klimov, V. I., Optical gain in colloidal quantum dots achieved with direct-current electrical pumping. *Nature materials* **2018**, *17* (1), 42-49.
- [6] Livache, C.; Martinez, B.; Goubet, N.; Gréboval, C.; Qu, J.; Chu, A.; Royer, S.; Ithurria, S.; Silly, M. G.; Dubertret, B., A colloidal quantum dot infrared photodetector and its use for intraband detection. *Nature communications* **2019**, *10* (1), 1-10.
- [7] Parrish, C. H.; Hebert, D.; Jackson, A.; Ramasamy, K.; McDaniel, H.; Giacomelli, G. A.; Bergren, M. R., Optimizing spectral quality with quantum dots to enhance crop yield in controlled environments. *Communications biology* **2021**, *4* (1), 1-9.
- [8] Sargent, E. H., Colloidal quantum dot solar cells. *Nature photonics* **2012**, *6* (3), 133-135.
- [9] Shirasaki, Y.; Supran, G. J.; Bawendi, M. G.; Bulović, V., Emergence of colloidal quantum-dot light-emitting technologies. *Nature photonics* **2013**, *7* (1), 13-23.
- [10] Wu, K.; Park, Y.-S.; Lim, J.; Klimov, V. I., Towards zero-threshold optical gain using charged semiconductor quantum dots. *Nature Nanotechnology* **2017**, *12* (12), 1140-1147.
- [11] Kwak, J.; Bae, W. K.; Lee, D.; Park, I.; Lim, J.; Park, M.; Cho, H.; Woo, H.; Yoon, D. Y.; Char, K., Bright and efficient full-color colloidal quantum dot light-emitting diodes using an inverted device structure. *Nano letters* **2012**, *12* (5), 2362-2366.
- [12] Lee, T.; Kim, B. J.; Lee, H.; Hahm, D.; Bae, W. K.; Lim, J.; Kwak, J., Bright and Stable Quantum Dot Light-Emitting Diodes. *Advanced Materials* **2022**, *34* (4), 2106276.

- [13] Sun, Q.; Wang, Y. A.; Li, L. S.; Wang, D.; Zhu, T.; Xu, J.; Yang, C.; Li, Y., Bright, multicoloured light-emitting diodes based on quantum dots. *Nature photonics* **2007**, *1* (12), 717-722.
- [14] Zhang, F.; Wang, S.; Wang, L.; Lin, Q.; Shen, H.; Cao, W.; Yang, C.; Wang, H.; Yu, L.; Du, Z., Super color purity green quantum dot light-emitting diodes fabricated by using CdSe/CdS nanoplatelets. *Nanoscale* **2016**, *8* (24), 12182-12188.
- [15] Brus, L., Electronic wave functions in semiconductor clusters: experiment and theory. *The Journal of Physical Chemistry* **1986**, *90* (12), 2555-2560.
- [16] Colvin, V. L.; Schlamp, M. C.; Alivisatos, A. P., Light-emitting diodes made from cadmium selenide nanocrystals and a semiconducting polymer. *Nature* **1994**, *370* (6488), 354-357.
- [17] Dai, X.; Zhang, Z.; Jin, Y.; Niu, Y.; Cao, H.; Liang, X.; Chen, L.; Wang, J.; Peng, X., Solution-processed, high-performance light-emitting diodes based on quantum dots. *Nature* **2014**, *515* (7525), 96-99.
- [18] Moon, H.; Chae, H., Efficiency enhancement of all-solution-processed inverted-structure green quantum dot light-emitting diodes via partial ligand exchange with thiophenol derivatives having negative dipole moment. *Advanced Optical Materials* **2020**, *8* (1), 1901314.
- [19] Song, J.; Wang, O.; Shen, H.; Lin, Q.; Li, Z.; Wang, L.; Zhang, X.; Li, L. S., Over 30% external quantum efficiency light-emitting diodes by engineering quantum dot-assisted energy level match for hole transport layer. *Advanced Functional Materials* **2019**, *29* (33), 1808377.
- [20] Lee, C.; Nam, E.; Lee, W.; Chae, H., Hydrosilylation of Reactive Quantum Dots and Siloxanes for Stable Quantum Dot Films. *Polymers* **2019**, *11* (5), 905.
- [21] Müller, J.; Lupton, J. M.; Rogach, A. L.; Feldmann, J.; Talapin, D. V.; Weller, H., Air-induced fluorescence bursts from single semiconductor nanocrystals. *Applied Physics Letters* **2004**, *85* (3), 381-383.
- [22] Pechstedt, K.; Whittle, T.; Baumberg, J.; Melvin, T., Photoluminescence of Colloidal CdSe/ZnS Quantum Dots: The Critical Effect of Water Molecules. *The Journal of Physical Chemistry C* **2010**, *114* (28), 12069-12077.
- [23] Deng, Y.; Lin, X.; Fang, W.; Di, D.; Wang, L.; Friend, R. H.; Peng, X.; Jin, Y., Deciphering exciton-generation processes in quantum-dot electroluminescence. *Nature Communications* **2020**, *11* (1), 2309.
- [24] Park, J.; Won, Y.-H.; Kim, T.; Jang, E.; Kim, D., Electrochemical Charging Effect on the Optical Properties of InP/ZnSe/ZnS Quantum Dots. *Small* **2020**, *16* (41), 2003542.
- [25] Park, Y.-S.; Bae, W. K.; Pietryga, J. M.; Klimov, V. I., Auger Recombination of Biexcitons and Negative and Positive Trions in Individual Quantum Dots. *ACS Nano* **2014**, *8* (7), 7288-7296.
- [26] Davidson-Hall, T.; Aziz, H., The role of excitons within the hole transporting layer in quantum dot light emitting device degradation. *Nanoscale* **2019**, *11* (17), 8310-8318.
- [27] Davidson-Hall, T.; Aziz, H., Significant Enhancement in Quantum Dot Light-Emitting Device Stability via a Cascading Hole Transport Layer. *ACS Appl Mater Interfaces* **2020**, *12* (14), 16782-16791.

- [28] Xue, X.; Dong, J.; Wang, S.; Zhang, H.; Zhang, H.; Zhao, J.; Ji, W., Degradation of quantum dot light emitting diodes, the case under a low driving level. *Journal of Materials Chemistry C* **2020**, *8* (6), 2014-2018.
- [29] Sun, Y.; Su, Q.; Zhang, H.; Wang, F.; Zhang, S.; Chen, S., Investigation on Thermally Induced Efficiency Roll-Off: Toward Efficient and Ultrabright Quantum-Dot Light-Emitting Diodes. *ACS Nano* **2019**, *13* (10), 11433-11442.
- [30] Yoshida, K.; Nakanotani, H.; Adachi, C., Effect of Joule heating on transient current and electroluminescence in p-i-n organic light-emitting diodes under pulsed voltage operation. *Organic Electronics* **2016**, *31*, 287-294.
- [31] Pu, C.; Dai, X.; Shu, Y.; Zhu, M.; Deng, Y.; Jin, Y.; Peng, X., Electrochemically-stable ligands bridge the photoluminescence-electroluminescence gap of quantum dots. *Nature Communications* **2020**, *11* (1), 937.
- [32] Jang, E.; Kim, Y.; Won, Y.-H.; Jang, H.; Choi, S.-M., Environmentally Friendly InP-Based Quantum Dots for Efficient Wide Color Gamut Displays. *ACS Energy Letters* **2020**, *5* (4), 1316-1327.
- [33] Kim, K.; Lee, H.; Ahn, J.; Jeong, S., Highly luminescing multi-shell semiconductor nanocrystals InP/ZnSe/ZnS. *Applied Physics Letters* **2012**, *101* (7), 073107.
- [34] Xie, R.; Battaglia, D.; Peng, X., Colloidal InP Nanocrystals as Efficient Emitters Covering Blue to Near-Infrared. *Journal of the American Chemical Society* **2007**, *129* (50), 15432-15433.
- [35] Won, Y.-H.; Cho, O.; Kim, T.; Chung, D.-Y.; Kim, T.; Chung, H.; Jang, H.; Lee, J.; Kim, D.; Jang, E., Highly efficient and stable InP/ZnSe/ZnS quantum dot light-emitting diodes. *Nature* **2019**, *575* (7784), 634-638.
- [36] Han, M. G.; Lee, Y.; Kwon, H.-i.; Lee, H.; Kim, T.; Won, Y.-H.; Jang, E., InP-based quantum dot light-emitting diode with a blended emissive layer. *ACS Energy Letters* **2021**, *6* (4), 1577-1585.
- [37] Chao, W.-C.; Chiang, T.-H.; Liu, Y.-C.; Huang, Z.-X.; Liao, C.-C.; Chu, C.-H.; Wang, C.-H.; Tseng, H.-W.; Hung, W.-Y.; Chou, P.-T., High efficiency green InP quantum dot light-emitting diodes by balancing electron and hole mobility. *Communications Materials* **2021**, *2* (1), 1-10.
- [38] Wang, Y.; Wu, Q.; Wang, L.; Sun, Z.; Cao, F.; Kong, L.; Li, L.; Zhang, C.; Wang, S.; Zhang, Z., Boosting the efficiency and stability of green InP quantum dot light emitting diodes by interface dipole modulation. *Journal of Materials Chemistry C* **2022**, *10* (21), 8192-8198.
- [39] Chen, B.; Li, D.; Wang, F., InP Quantum Dots: Synthesis and Lighting Applications. *Small* **2020**, *16* (32), e2002454.
- [40] Liu, P.; Lou, Y.; Ding, S.; Zhang, W.; Wu, Z.; Yang, H.; Xu, B.; Wang, K.; Sun, X. W., Green InP/ZnSeS/ZnS Core Multi-Shelled Quantum Dots Synthesized with Aminophosphine for Effective Display Applications. *Advanced Functional Materials* **2021**, *31* (11).
- [41] Reiss, P.; Carriere, M.; Lincheneau, C.; Vaure, L.; Tamang, S., Synthesis of Semiconductor Nanocrystals, Focusing on Nontoxic and Earth-Abundant Materials. *Chem Rev* **2016**, *116* (18), 10731-819.

- [42] Tessier, M. D.; Baquero, E. A.; Dupont, D.; Grigel, V.; Bladt, E.; Bals, S.; Coppel, Y.; Hens, Z.; Nayral, C.; Delpech, F., Interfacial Oxidation and Photoluminescence of InP-Based Core/Shell Quantum Dots. *Chemistry of Materials* **2018**, *30* (19), 6877-6883.
- [43] Ko, D.; Lee, J., 69-1: Invited Paper: Trap-dependent Electrical Characteristics of Organic Semiconductor Devices. *SID Symposium Digest of Technical Papers* **2020**, *51* (1), 2121-2124.
- [44] Le Corre, V. M.; Duijnste, E. A.; El Tambouli, O.; Ball, J. M.; Snaith, H. J.; Lim, J.; Koster, L. J. A., Revealing Charge Carrier Mobility and Defect Densities in Metal Halide Perovskites via Space-Charge-Limited Current Measurements. *ACS Energy Letters* **2021**, *6* (3), 1087-1094.
- [45] Shi, D.; Adinolfi, V.; Comin, R.; Yuan, M.; Alarousu, E.; Buin, A.; Chen, Y.; Hoogland, S.; Rothenberger, A.; Katsiev, K.; Losovyj, Y.; Zhang, X.; Dowben, P. A.; Mohammed, O. F.; Sargent, E. H.; Bakr, O. M., Low trap-state density and long carrier diffusion in organolead trihalide perovskite single crystals. *Science* **2015**, *347* (6221), 519-522.
- [46] Asokan, S.; Krueger, K. M.; Colvin, V. L.; Wong, M. S., Shape-Controlled Synthesis of CdSe Tetrapods Using Cationic Surfactant Ligands. *Small* **2007**, *3* (7), 1164-1169.
- [47] Green, M., The nature of quantum dot capping ligands. *Journal of Materials Chemistry* **2010**, *20* (28), 5797-5809.
- [48] Heuer-Jungemann, A.; Feliu, N.; Bakaimi, I.; Hamaly, M.; Alkilany, A.; Chakraborty, I.; Masood, A.; Casula, M. F.; Kostopoulou, A.; Oh, E.; Susumu, K.; Stewart, M. H.; Medintz, I. L.; Stratakis, E.; Parak, W. J.; Kanaras, A. G., The Role of Ligands in the Chemical Synthesis and Applications of Inorganic Nanoparticles. *Chemical Reviews* **2019**, *119* (8), 4819-4880.
- [49] Liu, Y.-F.; Yu, J.-S., Selective synthesis of CdTe and high luminescence CdTe/CdS quantum dots: The effect of ligands. *Journal of Colloid and Interface Science* **2009**, *333* (2), 690-698.
- [50] Inerbaev, T. M.; Masunov, A. E.; Khondaker, S. I.; Dobrinescu, A.; Plamadă, A.-V.; Kawazoe, Y., Quantum chemistry of quantum dots: Effects of ligands and oxidation. *The Journal of chemical physics* **2009**, *131* (4), 044106.
- [51] Kirkwood, N.; Monchen, J. O.; Crisp, R. W.; Grimaldi, G.; Bergstein, H. A.; Du Fossé, I.; Van Der Stam, W.; Infante, I.; Houtepen, A. J., Finding and fixing traps in II–VI and III–V colloidal quantum dots: the importance of Z-type ligand passivation. *Journal of the American Chemical Society* **2018**, *140* (46), 15712-15723.
- [52] Straus, D. B.; Goodwin, E. D.; Gaulding, E. A.; Muramoto, S.; Murray, C. B.; Kagan, C. R., Increased Carrier Mobility and Lifetime in CdSe Quantum Dot Thin Films through Surface Trap Passivation and Doping. *The Journal of Physical Chemistry Letters* **2015**, *6* (22), 4605-4609.
- [53] Bohm, M. L.; Jellicoe, T. C.; Rivett, J. P.; Sadhanala, A.; Davis, N. J.; Morgenstern, F. S.; Godel, K. C.; Govindasamy, J.; Benson, C. G.; Greenham, N. C., Size and energy level tuning of quantum dot solids via a hybrid ligand complex. *The Journal of Physical Chemistry Letters* **2015**, *6* (17), 3510-3514.

- [54] Brown, P. R.; Kim, D.; Lunt, R. R.; Zhao, N.; Bawendi, M. G.; Grossman, J. C.; Bulovic, V., Energy level modification in lead sulfide quantum dot thin films through ligand exchange. *ACS nano* **2014**, *8* (6), 5863-5872.
- [55] Jasieniak, J.; Califano, M.; Watkins, S. E., Size-dependent valence and conduction band-edge energies of semiconductor nanocrystals. *ACS nano* **2011**, *5* (7), 5888-5902.
- [56] Park, Y.; Klöckner, B.; Hahm, D.; Kim, J.; Lee, T.; Kim, J.; Bae, W. K.; Zentel, R.; Kwak, J., Origin of enhanced efficiency and stability in diblock copolymer-grafted Cd-free quantum dot-based light-emitting diodes. *Journal of Materials Chemistry C* **2021**, *9* (32), 10398-10405.
- [57] Saha, S.; Sarkar, S.; Pal, S.; Sarkar, P., Ligand mediated tuning of the electronic energy levels of ZnO nanoparticles. *RSC advances* **2013**, *3* (2), 532-539.
- [58] Shulenberg, K. E.; Keller, H. R.; Pellows, L. M.; Brown, N. L.; Dukovic, G., Photocharging of Colloidal CdS Nanocrystals. *The Journal of Physical Chemistry C* **2021**, *125* (41), 22650-22659.
- [59] Zeng, Y.; Kelley, D. F., Excited hole photochemistry of CdSe/CdS quantum dots. *The Journal of Physical Chemistry C* **2016**, *120* (31), 17853-17862.
- [60] Pu, C.; Peng, X., To battle surface traps on CdSe/CdS core/shell nanocrystals: shell isolation versus surface treatment. *Journal of the American Chemical Society* **2016**, *138* (26), 8134-8142.
- [61] Shen, Y.; Tan, R.; Gee, M. Y.; Greytak, A. B., Quantum yield regeneration: influence of neutral ligand binding on photophysical properties in colloidal core/shell quantum dots. *ACS nano* **2015**, *9* (3), 3345-3359.
- [62] Liu, M.; Wang, Y.-Y.; Liu, Y.; Jiang, F.-L., Thermodynamic implications of the ligand exchange with alkylamines on the surface of CdSe quantum dots: The importance of ligand–ligand interactions. *The Journal of Physical Chemistry C* **2020**, *124* (8), 4613-4625.
- [63] Anderson, N. C.; Hendricks, M. P.; Choi, J. J.; Owen, J. S., Ligand exchange and the stoichiometry of metal chalcogenide nanocrystals: spectroscopic observation of facile metal-carboxylate displacement and binding. *Journal of the American Chemical Society* **2013**, *135* (49), 18536-18548.
- [64] Ritchhart, A.; Cossairt, B. M., Quantifying ligand exchange on InP using an atomically precise cluster platform. *Inorganic Chemistry* **2019**, *58* (4), 2840-2847.
- [65] Wei, S.; Peng, J.; Wang, M.; Fang, X.; Fan, Y.; Li, X.; Lu, J., The (Zn_{0.95}Mn_{0.05}S)₂·L (L= hexylamine and octylamine) inorganic/organic hybrid luminescence films by a spin-coating method. *Chemical Communications* **2012**, *48* (38), 4615-4617.
- [66] Baek, G. W.; Seo, S. G.; Hahm, D.; Bae, W. K.; Kwak, J.; Jin, S. H., Highly Efficient, Surface Ligand Modified Quantum Dot Light-Emitting Diodes Driven by Type-Controllable MoTe₂ Thin Film Transistors via Electron Charge Enhancer. *Advanced Electronic Materials* **2021**, *7* (10), 2100535.

Publication

[1] International Journals

1. Kim, J.*; Jung, H.; Song, J.; **Kim, K.**; Lee, C., Analysis of Interfacial Layer-Induced Open-Circuit Voltage Burn-In Loss in Polymer Solar Cells on the Basis of Electroluminescence and Impedance Spectroscopy., *ACS applied materials & interfaces*, **2017**, 9 (28), 24052-24060.
2. Rhee, S.*; Chang, J. H*.; Hahm, D.; **Kim, K.**; Jeong, B. G.; Lee, H. J.; Lim, J.; Char, K.; Lee, C.; Bae, W. K., “Positive incentive” approach to enhance the operational stability of quantum dot-based light-emitting diodes., *ACS applied materials & interfaces*, **2019**, 11 (43), 40252-40259.
3. Lee, T.*; Hahm, D.; **Kim, K.**; Bae, W. K.; Lee, C.; Kwak, J., Highly efficient and bright inverted top-emitting InP quantum dot light-emitting diodes introducing a hole-suppressing interlayer., *Small*, **2019**, 15 (50), 1905162.
4. Yang, J.*; Hahm, D.*; **Kim, K.***; Rhee, S.; Lee, M.; Kim, S.; Chang, J. H.; Park, H. W.; Lim, J.; Lee, M.; Kim, H.; Bang, J.; Ahn, H.; Cho, J. H.; Kwak, J.; Kim, B.; Lee, C.; Bae, W. K.; Kang, M. S., High-resolution patterning of colloidal quantum dots via non-destructive, light-driven ligand crosslinking. *Nature communications* **2020**, 11 (1), 2874.
5. Rhee, S.*; **Kim, K.**; Roh, J.; Kwak, J., Recent progress in high-luminance quantum dot light-emitting diodes., *Current Optics and Photonics*, **2020**, 4 (3),

161-173.

6. Kim, S. H.*; Baek, G. W.*; Yoon, J.; Seo, S.; Park, J.; Hahm, D.; Chang, J. H.; Seong, D.; Seo, H.; Oh, S.; **Kim, K.**; Jung, H.; Oh, Y.; Baac, H. W.; Alimkhanuly, B.; Bae, W. K.; Lee, S.; Lee, M.; Kwak, J.; Park, J.-H.; Son, D., A Bioinspired Stretchable Sensory-Neuromorphic System., *Advanced Materials*, **2021**, 33 (44), 2104690.
7. **Kim, K.***; Hahm, D.; Baek, G. W.; Lee, T.; Shin, D.; Lim, J.; Bae, W. K.; Kwak, J., Effect of Excess Carriers on the Degradation of InP-Based Quantum-Dot Light-Emitting Diodes. *ACS Applied Electronic Materials*, **2022**, 4 (12), 6229-6236.

[2] International Conferences

1. **K Kim**, H Jung and C. Lee, “Increasing transfer yield of contact imprinting process for high resolution quantum dot light-emitting diodes”, The 17th International Meeting on Information Display, Busan, Korea (Aug, 2017). (Poster)
2. **K Kim**, H Jung and C. Lee, “Increasing efficiency of Quantum-dot Light Emitting Diodes which fabricated by contact imprinting process”, 8th International Conference on Flexible and Printed Electronics, Jeju, Korea (Sep, 2017). (Poster)
3. **K Kim**, H Jung and C. Lee, “Effect of Solvents and Pressure on the Performance of Quantum Dot light Emitting Diodes Fabricated with Soft-Contact Transfer Printing”, Society for Information Display – Display Week 2018, Los Angeles, CA, US (May, 2018). (Poster)

4. **K Kim**, H Jung, WK Bae and C. Lee, “Effect of Pressure and solvent on formation of Quantum dots film for soft contact printing”, The 18th International Meeting on Information Display, Busan, Korea (Aug, 2018). (Poster)
5. **K Kim**, T Lee, D Hahm, WK Bae and J Kwak, “Highly bright cadmium-free QLEDs using alkylamine ligands”, The 19th International Meeting on Information Display, Gyeongju, Korea (Aug, 2019). (Poster)
6. **K Kim** and J Kwak, “Analysis on the degradation of Cd-free InP based quantum dot light-emitting diode”, The 21th International Meeting on Information Display, Seoul, Korea (Aug, 2021). (Oral)

한글 초록

최근 조명 및 디스플레이 응용 분야를 위한 콜로이드 양자점 발광 다이오드에 대한 관심이 양자점의 고순도, 색상 제어의 용이성 및 공정 단순성 등 뛰어난 특성으로 인해 증가하고 있다. 수년 동안 양자점 발광 다이오드의 소자 성능은 재료 합성, 전기 물리 분석 및 소자 설계에 대한 여러 연구에 의해 향상되었다. 하지만 성능에 발전에 따라 양자점 재료가 가지는 중금속에 대한 환경문제가 제기되었고 중금속을 포함하지 않는 친환경 소재 및 그 소자에 대한 많은 연구가 진행되고 있다. 중금속이 없는 양자점의 성능이 향상됨에 따라 작동 중 열화 메커니즘에 대한 이해가 안정적인 소자 제작을 위한 중요한 문제가 되고 있다. 중금속이 없는 양자점 발광 다이오드의 효율 향상에 대한 수많은 보고에도 불구하고 휘도 저하의 메커니즘은 아직 충분히 규명되지 않았다.

이를 밝히기 위해, 하이브리드 역 구조를 갖는 인화인듐 기반 양자점 발광 다이오드의 휘도 감소를 분석하였다. 전기적 구동 중, 전자와 정공이 각각 휘도 감소에 미치는 영향을 분류하기 위해 의도적으로 전하가 불균형하게 주입되는 소자를 제작하였으며 전하 불균형 소자를 만들기 위해 양자점 층 도포 전후 절연층을 삽입하였다. 이와 더불어 휘도 감소의 특성을 구동 중에만 발생하는 일시적인 가역적 휘도 감소와 구동 후에도 회복되지 않는 비가역적 휘도 감소로 나누어 측정하였다. 가역적 요인 측면에서는 과도한 전자 주입에 의한 비방사성 오제 재결합이 주요

원인으로 고려되었으며 이는 전기적 구동 후 소자 내 방전 과정을 거쳐 다시 회복될 수 있는 일시적인 요인임을 확인하였다. 반면에 과도한 정공 주입은 일시적인 휘도 감소에 영향을 미치지 않고 양자점 내 영구적으로 트랩 사이트를 형성하여 비가역적인 휘도 저하를 야기함으로써 방전 과정 후에도 휘도가 회복되지 않았다. 결론적으로, 각각의 과잉 캐리어는 다른 메커니즘으로 초기 단계 장치 성능 저하를 일으킬 수 있음을 확인하였다.

양자점의 전기적 안정성이 정공 과다상태에서 크게 감소한다는 사실을 기반으로 상대적으로 안정하다고 알려진 아민 리간드 치환을 통해 양자점 표면을 처리하여 소자의 안정성을 크게 향상시켰다. 양자점 표면의 리간드의 역할은 합성 과정을 제어하고 양자점을 콜로이드 상태로 만들 뿐만 아니라 표면의 전기적 특성에도 영향을 미친다. 본 실험에서는 양자점 표면에 부착된 올레산 리간드를 제거하고 상대적으로 짧은 헥실아민 리간드를 치환하였다. 리간드 치환 후 자외선광전자분광 측정을 통해 양자점 에너지 준위가 상향 이동함을 확인하였다. 그리고 전자와 정공만 흐르게 조절한 소자에서 전자 주입은 약간 감소하고 정공 주입이 4 배 증가하였다. 그 결과, 리간드 치환을 통해 스펙트럼을 변화시키지 않고 향상된 정공 주입 효과로 인해 양자점 발광 다이오드의 전류 밀도 및 휘도가 증가하고 전류 증가에 따른 효율 감소가 향상되었다. 또한, 동작 중 캐리어 축적으로 인한 영향이 감소함을 확인하였고, 열화 전후에 영구 휘도 감소의 원인이 감소됨을 확인하였다. 무엇보다도 인화인듐 양자점 열화원인으로 예상되었던 정공에 의한 리간드 분리가 크게 개선되어 앞서 원인과 더불어 양자점 발광 다이오드의 안정성을 크게 증가시킬 수 있었을 뿐 더러 인화 인듐 녹색 QD 에 적용했을 때 적색과

마찬가지로 소자의 안정성이 크게 향상되어 구동 중, 인화인듐 양자점의 열화가 소자 수명에 큰 영향을 미치고 리간드 치환 방법이 범용적으로 사용될 수 있음을 증명하였다.

본 논문에서는 인화인듐 양자점 발광다이오드의 초기 열화와 리간드 치환을 통해 일어나는 현상을 연구하였다. 우리의 연구는 고안정성 비중금속 기반 QLED 개발에 기여할 수 있다.

주요어: 양자점 발광다이오드, 리간드 치환, 인화 인듐 양자점, 소자 구동 안정성

학번: 2016-20867